

Sigma-Point Kalman Filters for Nonlinear Estimation and Sensor-Fusion - Applications to Integrated Navigation -

Rudolph van der Merwe* and Eric A. Wan†

OGI School of Science & Engineering, Oregon Health & Science University, Beaverton, OR 97006

Simon I. Julier‡

IDAK Industries, Washington DC.

Nonlinear estimation based on probabilistic inference forms a core component in most modern GNC systems. The estimator optimally fuses observations from multiple sensors with predictions from a nonlinear dynamic state-space model of the system under control. The current industry standard and most widely used algorithm for this purpose is the extended Kalman filter (EKF). Unfortunately, the EKF is based on a sub-optimal implementation of the recursive Bayesian estimation framework applied to Gaussian random variables. This can seriously affect the accuracy or even lead to divergence of the system. In this paper, we apply a new probabilistic framework, called Sigma-point Kalman Filters (SPKF), to the same problem domain typically addressed by the EKF. SPKF methods have proven to be far superior to standard EKF based estimation approaches in a wide range of applications. Whereas the EKF can be viewed as a first-order method for dealing with nonlinearities, an SPKF achieves second-order or higher accuracy. Remarkably, the computational complexity of a SPKF is of the same order as the EKF. Furthermore, implementation of the SPKF is often substantially easier and requires no analytic derivation or Jacobians as in the EKF.

In this paper, we review the fundamental development of the SPKF family of algorithms. These include specific variants such as the unscented Kalman filter (UKF),¹ the central-difference Kalman filter (CDKF),² and numerically efficient and stable square-root implementations.³⁻⁵ We also introduce a novel SPKF based method to fuse latency lagged observations in a theoretically consistent fashion.

In the second part of the paper, we focus on the application of the SPKF to the integrated navigation problem as it relates to unmanned aerial vehicle (UAV) autonomy. We specifically detail the development of a loosely coupled implementation for integrating GPS measurements with an inertial measurement unit (IMU) and altimeter. The SPKF-based sensor latency compensation technique mentioned above is used to accurately fuse the lagged GPS measurements. A UAV (helicopter) test platform is used to demonstrate the results. Performance metrics indicate an approximate 30% error reduction in both attitude and position estimates relative to the baseline EKF implementation.

I. Introduction

A central and vital operation performed in all Kalman filters is the propagation of a Gaussian random variable (GRV) through the system dynamics. In the EKF, the system state distribution and all relevant noise densities are approximated by GRVs, which are then propagated analytically through a first-order linearization of the nonlinear system. This can introduce large errors in the true posterior mean and covariance

*Senior Research Associate, Adaptive Systems Lab, CSE Department, OGI - OHSU, 20000 NW Walker Rd., Beaverton, OR 97006, rudmerwe@cse.ogi.edu

†Associate Professor, Adaptive Systems Lab, CSE Department, OGI - OHSU, 20000 NW Walker Rd., Beaverton, OR 97006, ericwan@cse.ogi.edu

‡IDAK Industries, Washington DC, sjulier@erols.com

of the transformed GRV, which may lead to sub-optimal performance and sometimes divergence of the filter. The SPKF addresses this problem by using a deterministic sampling approach. The state distribution is again approximated by a GRV, but is now represented using a minimal set of carefully chosen weighted sample points. These sample points completely capture the true mean and covariance of the GRV, and when propagated through the true nonlinear system, captures the posterior mean and covariance accurately to the 2nd order (Taylor series expansion) for any nonlinearity. The EKF, in contrast, only achieves first-order accuracy. Remarkably, the computational complexity of the SPKF is the same order as that of the EKF. Furthermore, implementation of the SPKF is often substantially easier and requires no analytic derivation or Jacobians as in the EKF. SPKF methods have proven to be far superior to standard EKF based estimation approaches in a wide range of applications in the areas of nonlinear state estimation, parameter estimation (system identification) as well as dual estimation (machine learning).⁶⁻⁸

In the first part of the paper we review the general state-estimation framework employed by all Kalman filters, after which we highlight the basic assumptions and flaws with using the EKF. We then introduce and review the fundamental development of the SPKF family of algorithms. This presentation is based on the general sigma-point approach for the calculation of the posterior statistics of a random variables that undergoes a nonlinear transformation. The actual algorithmic specification of different SPKF variants such as the *unscented Kalman filter* (UKF),¹ *central difference Kalman filter* (CDKF),² and numerically efficient and stable square-root implementations^{3,4} are deferred to the appendices at the end of this paper. A number of examples are provided to illustrate the difference in performance between the EKF and SPKF. We also introduce a novel SPKF based method to fuse latency lagged observations. Previous approaches using the EKF have a high computational cost and can be highly inaccurate due to nonlinearities.⁹

In the second part of the paper, we focus on the application of the SPKF to the integrated navigation problem. In a typical integrated GPS/INS system, an EKF combines rate-gyro and accelerometer data (from an IMU) with a kinematic or dynamic model of a vehicle movement. Other sensors such as barometric altimeter or magnetic compass may also be integrated. GPS position and velocity measurements are then used to correct INS errors using the same EKF. The navigational state of the vehicle to be estimated include position, attitude, velocities, as well as INS sensor biases. In addition (for loosely coupled implementations), the GPS receiver may employ its own EKF to solve position and velocity estimates (and timing) from satellite pseudorange, phase, and Doppler data. Alternatively, in a tightly coupled approach, a single EKF may be used to combine raw satellite signals with the IMU and other sensor measurements to make an optimal estimation of the vehicles navigational state. We specifically detail the development of a loosely coupled implementation for integrating GPS measurements with an IMU and altimeter within the context of autonomous UAV guidance, navigation and control. The use of the SPKF directly replaces the EKF. We report experimental results generated using both a high-fidelity UAV simulation system (for ground truth comparison) as well as on real flight data using a fully instrumented XCell-90 RC helicopter platform.

II. The EKF and its Flaws

The general Kalman framework involves estimation of the state of a discrete-time nonlinear dynamic system,

$$\mathbf{x}_{k+1} = \mathbf{f}(\mathbf{x}_k, \mathbf{v}_k) \quad (1)$$

$$\mathbf{y}_k = \mathbf{h}(\mathbf{x}_k, \mathbf{n}_k) \quad (2)$$

where \mathbf{x}_k represent the unobserved state of the system and \mathbf{y}_k is the only observed signal. The *process* noise \mathbf{v}_k drives the dynamic system, and the *observation* noise is given by \mathbf{n}_k . Note that we are not assuming additivity of the noise sources. The system dynamic model $\mathbf{f}(\cdot)$ and $\mathbf{h}(\cdot)$ are assumed known. In state-estimation, the EKF is the standard method of choice to achieve a recursive (approximate) maximum-likelihood estimation of the state \mathbf{x}_k . Given the noisy observation \mathbf{y}_k , the recursive estimation for \mathbf{x}_k can be expressed in the following form:¹⁰

$$\hat{\mathbf{x}}_k = \hat{\mathbf{x}}_k^- + \mathbf{K}_k (\mathbf{y}_k - \hat{\mathbf{y}}_k^-) \quad (3)$$

$$\mathbf{P}_{\mathbf{x}_k} = \mathbf{P}_{\mathbf{x}_k}^- - \mathbf{K}_k \mathbf{P}_{\tilde{\mathbf{y}}_k} \mathbf{K}_k^T \quad (4)$$

where $\hat{\mathbf{x}}_k^-$ is the *optimal prediction* of the state at time k conditioned on all of the observed information up to and including time $k - 1$, and $\hat{\mathbf{y}}_k^-$ is the *optimal prediction* of the observation at time k . $\mathbf{P}_{\mathbf{x}_k}^-$ is the

covariance of $\hat{\mathbf{x}}_k^-$, and $\mathbf{P}_{\hat{\mathbf{y}}_k}$ is the covariance of $\tilde{\mathbf{y}}_k = \mathbf{y}_k - \hat{\mathbf{y}}_k^-$, termed the *innovation*. The optimal terms in this recursion are given by

$$\hat{\mathbf{x}}_k^- = E[\mathbf{f}(\hat{\mathbf{x}}_{k-1}, \mathbf{v}_{k-1})] \quad (5)$$

$$\hat{\mathbf{y}}_k^- = E[\mathbf{h}(\hat{\mathbf{x}}_k^-, \mathbf{n}_k)] \quad (6)$$

$$\mathbf{K}_k = \mathbf{P}_{\mathbf{x}_k \mathbf{y}_k} \mathbf{P}_{\hat{\mathbf{y}}_k}^{-1} = E[(\mathbf{x}_k - \hat{\mathbf{x}}_k^-)(\mathbf{y}_k - \hat{\mathbf{y}}_k^-)^T] \times E[(\mathbf{y}_k - \hat{\mathbf{y}}_k^-)(\mathbf{y}_k - \hat{\mathbf{y}}_k^-)^T]^{-1} \quad (7)$$

where the optimal prediction $\hat{\mathbf{x}}_k^-$ corresponds to the expectation of a nonlinear function of the random variables $\hat{\mathbf{x}}_{k-1}$ and \mathbf{v}_{k-1} (see Eq. (5)). Similar interpretation holds for the optimal prediction of the observation $\hat{\mathbf{y}}_k^-$ in Eq. (6). The optimal gain term \mathbf{K}_k is expressed as a function of posterior covariance matrices in Eq. (7). Note these terms also require taking expectations of a nonlinear function of the prior state estimate RVs. This recursion provides the optimal minimum mean-squared error (MMSE) linear estimator of \mathbf{x}_k assuming all relevant random variables in the system can be efficiently and consistently modeled by maintaining their first and second order moments, i.e., they can be accurately modeled as Gaussian random variables (GRVs). We need not assume linearity of the system model $\mathbf{f}(\cdot)$ and $\mathbf{h}(\cdot)$.

The Kalman filter calculates the optimal quantities in Eqs. (5), (6) and (7) exactly in the linear case, and can be viewed as an efficient method for analytically propagating a GRV through linear system dynamics. For nonlinear models, however, the extended Kalman filter (EKF) approximates the optimal terms as:

$$\hat{\mathbf{x}}_k^- \approx \mathbf{f}(\hat{\mathbf{x}}_{k-1}, \bar{\mathbf{v}}) \quad (8)$$

$$\hat{\mathbf{y}}_k^- \approx \mathbf{h}(\hat{\mathbf{x}}_k^-, \bar{\mathbf{n}}) \quad (9)$$

$$\mathbf{K}_k \approx \hat{\mathbf{P}}_{\mathbf{x}_k \mathbf{y}_k}^{lin} \left(\hat{\mathbf{P}}_{\hat{\mathbf{y}}_k}^{lin} \right)^{-1} \quad (10)$$

where predictions are approximated as simply the function of the prior *mean* value for estimates (no expectation taken). The noise means are denoted by $\bar{\mathbf{v}}$ and $\bar{\mathbf{n}}$, and are usually assumed to equal to zero. The covariances are determined by linearizing the dynamic equations

$$\mathbf{x}_{k+1} \approx \mathbf{F}\mathbf{x}_k + \mathbf{B}\mathbf{v}_k \quad (11)$$

$$= [\nabla_{\mathbf{x}_k} \mathbf{f}(\mathbf{x}, \mathbf{v})] \mathbf{x}_k + [\nabla_{\mathbf{v}_k} \mathbf{f}(\mathbf{x}, \mathbf{v})] \mathbf{v}_k \quad (12)$$

$$\mathbf{y}_k \approx \mathbf{H}\mathbf{x}_k + \mathbf{D}\mathbf{n}_k \quad (13)$$

$$= [\nabla_{\mathbf{x}_k} \mathbf{h}(\mathbf{x}, \mathbf{n})] \mathbf{x}_k + [\nabla_{\mathbf{n}_k} \mathbf{h}(\mathbf{x}, \mathbf{n})] \mathbf{n}_k \quad (14)$$

and then determining (approximating) the posterior covariance matrices analytically for the linear system, i.e.,

$$\hat{\mathbf{P}}_{\mathbf{x}_k}^{lin} = \mathbf{F}\mathbf{P}_{\mathbf{x}_{k-1}}\mathbf{F}^T + \mathbf{B}\mathbf{Q}_{k-1}\mathbf{B}^T \quad (15)$$

$$\hat{\mathbf{P}}_{\mathbf{x}_k \mathbf{y}_k}^{lin} = \hat{\mathbf{P}}_{\mathbf{x}_k}^{lin} \mathbf{H}^T \quad (16)$$

$$\hat{\mathbf{P}}_{\hat{\mathbf{y}}_k}^{lin} = \mathbf{H}\hat{\mathbf{P}}_{\mathbf{x}_k}^{lin} \mathbf{H}^T + \mathbf{D}\mathbf{R}_k\mathbf{D}^T, \quad (17)$$

where $\mathbf{P}_{\mathbf{x}_{k-1}}$ is the posterior covariance of the state estimate at time $k-1$, \mathbf{Q} is the covariance matrix of the process noise and \mathbf{R} is the covariance matrix of the observation noise. In other words, in the EKF the state distribution is approximated by a GRV, which is then propagated analytically through the first-order linearization of the nonlinear system. This is equivalent to applying the linear Kalman filter covariance update equations to the linearized system. As such, the EKF can be viewed as providing “first-order” approximations to the optimal terms in Eq. (3). As mentioned earlier, these approximations used in the EKF can result in large errors in the estimates and even divergence of the filter.

III. The Sigma-Point Kalman Filter

The *sigma-point Kalman filter* address the approximation issues of the EKF. This is achieved through a fundamentally different approach for calculating the posterior 1st and 2nd order statistics of a random variable that undergoes a nonlinear transformation. The state distribution is again represented by a GRV,

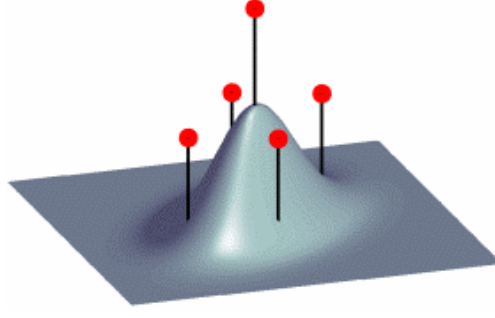


Figure 1. Weighted sigma-points for a 2 dimensional Gaussian random variable (RV). These sigma-points lie along the major eigen-axes of the RV's covariance matrix and complete captures the first and second order statistics of the RV. The height of each sigma-point indicates its relative weight.

but is now specified using a minimal set of deterministically chosen weighted sample points (See Fig. 1). These samples, called *sigma-points*, completely capture the true mean and covariance of the prior random variable, and when propagated through the *true* nonlinear system, captures the posterior mean and covariance accurately to the 2nd order (Taylor series expansion) for *any* nonlinearity (3rd order accuracy is achieved if the prior random variable has a symmetric distribution, such as the exponential family of pdfs.) The basic *sigma-point approach* (SPA) can be described as follows:^{1,5}

The Sigma-point Approach (SPA)

1. A set of weighted samples (*sigma-points*) are deterministically calculated using the mean and square-root decomposition of the covariance matrix of the prior random variable. As a minimal requirement the sigma-point set must completely capture the first and second order moments of the prior random variable. Higher order moments can be captured, if so desired, at the cost of using more sigma-points.
2. The sigma-points are propagated through the true nonlinear function using functional evaluations alone, i.e., no analytical derivatives are used, in order to generate a posterior sigma-point set.
3. The posterior statistics are calculated (approximated) using tractable functions of the the propagated sigma-points and weights. Typically these take on the form of simple weighted sample mean and covariance calculations of the posterior sigma-points.

To be more specific: Consider propagating a random variable $\mathbf{x} \in \mathbb{R}^L$ through an arbitrary nonlinear function $\mathbf{y} = \mathbf{g}(\mathbf{x})$. Assume \mathbf{x} has mean $\bar{\mathbf{x}}$ and covariance $\mathbf{P}_{\mathbf{x}}$. To calculate the statistics of \mathbf{y} , we form a set of $2L + 1$ sigma-points $\{\mathcal{X}_i; i=0, \dots, 2L\}$ where $\mathcal{X}_i \in \mathbb{R}^L$. The sigma-points are calculated using the following general selection scheme:

$$\begin{aligned} \mathcal{X}_0 &= \bar{\mathbf{x}} \\ \mathcal{X}_i &= \bar{\mathbf{x}} + \zeta (\sqrt{\mathbf{P}_{\mathbf{x}}})_i \quad i=1, \dots, L \\ \mathcal{X}_i &= \bar{\mathbf{x}} - \zeta (\sqrt{\mathbf{P}_{\mathbf{x}}})_i \quad i=L+1, \dots, 2L \end{aligned} \tag{18}$$

where ζ is a scalar scaling factor that determines the spread of the sigma-points around $\bar{\mathbf{x}}$ and $(\sqrt{\mathbf{P}})_i$ indicates the i th column of the matrix square-root of the covariance matrix \mathbf{P} . Once the sigma-points are calculated from the prior statistics as shown above, they are propagated through the nonlinear function,

$$\mathcal{Y}_i = \mathbf{g}(\mathcal{X}_i) \quad i=0, \dots, 2L \tag{19}$$

and the mean and covariance of \mathbf{y} are approximated using a weighted sample mean and covariance of the posterior sigma-points,

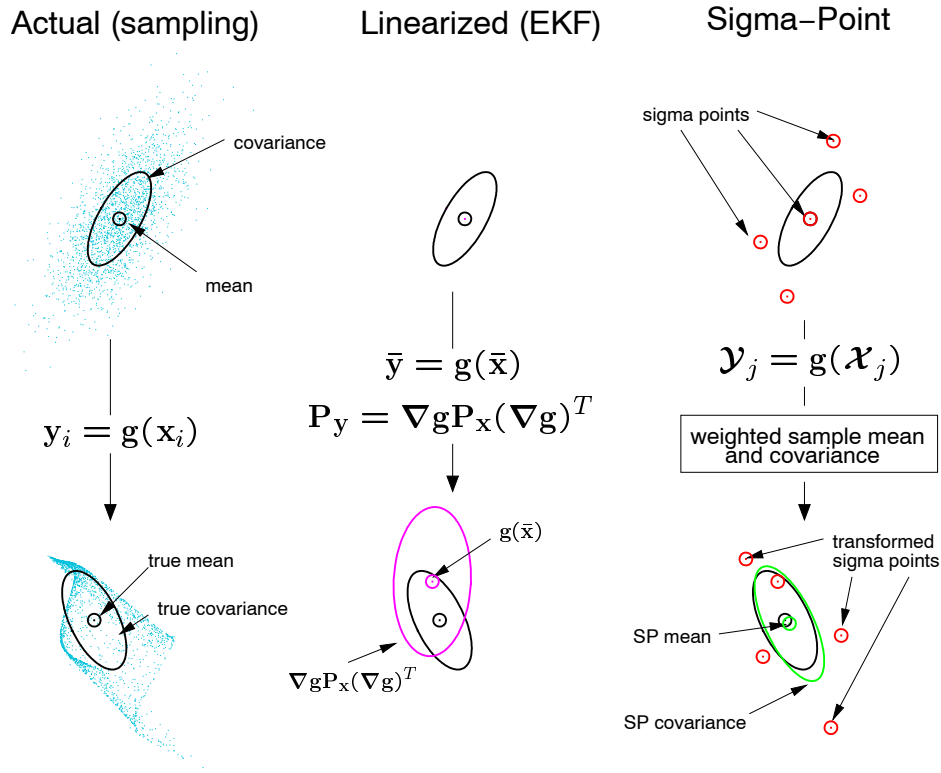


Figure 2. 2D example of sigma-point approach.

$$\bar{\mathbf{y}} \approx \sum_{i=0}^{2L} w_i^m \mathbf{y}_i \quad (20)$$

$$\mathbf{P}_y \approx \sum_{i=0}^{2L} \sum_{j=0}^{2L} w_{ij}^c \mathbf{y}_i \mathbf{y}_j^T \quad (21)$$

$$\mathbf{P}_{xy} \approx \sum_{i=0}^{2L} \sum_{j=0}^{2L} w_{ij}^c \mathbf{x}_i \mathbf{y}_j^T, \quad (22)$$

where w_i^m and w_{ij}^c are scalar weights. Note, all weights need not be positive valued. In fact, depending on the specific sigma-point approach at hand, certain weights on the cross-terms are set equal to zero, i.e., $w_{ij} = 0$ for certain $\{i, j; i \neq j\}$. The specific values of the weights (w) and the scaling factors (ζ) depend on the *type* of sigma-point approach used: These include the *unscented transformation*¹ and the Stirling-interpolation based *central difference transformation*² to name but two.

Note that the sigma-point approach differs substantially from general stochastic sampling techniques such as Monte-Carlo integration which require orders of magnitude more sample points in an attempt to propagate an accurate (possibly non-Gaussian) distribution of the state. The deceptively simple sigma-point approach results in posterior approximations that are accurate to the third order for Gaussian inputs for all nonlinearities. For non-Gaussian inputs, approximations are accurate to at least the second-order, with the accuracy of third and higher order moments determined by the specific choice of weights and scaling factors.⁵ Furthermore, no analytical Jacobians of the system equations need to be calculated as is the case for the EKF. This makes the sigma-point approach very attractive for use in “black box” systems where analytical expressions of the system dynamics are either not available or not in a form which allows for easy linearization.

A simple comparative example of the sigma-point approach is shown in Figure 2 for a 2-dimensional system: the left plot shows the true mean and covariance propagation using Monte Carlo sampling; the center plots show the results using a linearization approach as would be done in the EKF; the right hand

plots show the performance of the sigma-point approach (note, only 5 sigma-points are needed for the 2D case). The superior performance of the sigma-point approach is clearly evident.

A. Implementing the SPKF Algorithm

The sigma-point Kalman filter is a straightforward extension of the sigma-point approach to the recursive estimation in Eqs. (3)-(7), where the state RV is redefined as the concatenation of the original state and noise variables: $\mathbf{x}_k^a = [\mathbf{x}_k^T \quad \mathbf{v}_k^T \quad \mathbf{n}_k^T]^T$. The sigma-point selection scheme (Equation 18) is applied to this new augmented state RV to calculate the corresponding sigma-point set, $\{\mathcal{X}_{k,i}^a; i=0,\dots,2L\}$ where $\mathcal{X}_{k,i}^a \in \mathbb{R}^{L_x+L_v+L_n}$. The pseudo-code for the SPKF is given below:

- *Initialization:*

$$\begin{aligned}\hat{\mathbf{x}}_0 &= E[\mathbf{x}_0] \quad , \quad \mathbf{P}_{\mathbf{x}_0} = E[(\mathbf{x}_0 - \hat{\mathbf{x}}_0)(\mathbf{x}_0 - \hat{\mathbf{x}}_0)^T] \\ \hat{\mathbf{x}}_0^a &= E[\mathbf{x}_0^a] = \begin{bmatrix} \hat{\mathbf{x}}_0^T & \bar{\mathbf{v}}_0^T & \bar{\mathbf{n}}_0^T \end{bmatrix}^T \\ \mathbf{P}_0^a &= E[(\mathbf{x}_0^a - \hat{\mathbf{x}}_0^a)(\mathbf{x}_0^a - \hat{\mathbf{x}}_0^a)^T] \\ &= \begin{bmatrix} \mathbf{P}_{\mathbf{x}_0} & \mathbf{0} & \mathbf{0} \\ \mathbf{0} & \mathbf{R}_v & \mathbf{0} \\ \mathbf{0} & \mathbf{0} & \mathbf{R}_n \end{bmatrix}\end{aligned}$$

- For $k = 1, \dots, \infty$:

1. Set $t = k - 1$
2. Calculate sigma-points:

$$\mathcal{X}_t^a = \begin{bmatrix} \hat{\mathbf{x}}_t^a & \hat{\mathbf{x}}_t^a + \zeta\sqrt{\mathbf{P}_t^a} & \hat{\mathbf{x}}_t^a - \zeta\sqrt{\mathbf{P}_t^a} \end{bmatrix}$$

3. Time-update equations:

$$\begin{aligned}\mathcal{X}_{k|t}^x &= \mathbf{f}(\mathcal{X}_t^x, \mathcal{X}_t^v, \mathbf{u}_t) \\ \hat{\mathbf{x}}_k^- &= \sum_{i=0}^{2L} w_i^m \mathcal{X}_{i,k|t}^x \\ \mathbf{P}_{\mathbf{x}_k}^- &= \sum_{i=0}^{2L} \sum_{j=0}^{2L} w_{ij}^c (\mathcal{X}_{i,k|t}^x - \hat{\mathbf{x}}_k^-) (\mathcal{X}_{j,k|t}^x - \hat{\mathbf{x}}_k^-)^T\end{aligned}$$

4. Measurement-update equations:

$$\begin{aligned}\mathcal{Y}_{k|t} &= \mathbf{h}(\mathcal{X}_{k|t}^x, \mathcal{X}_t^n) \\ \hat{\mathbf{y}}_k^- &= \sum_{i=0}^{2L} w_i^m \mathcal{Y}_{i,k|t} \\ \mathbf{P}_{\mathbf{y}_k} &= \sum_{i=0}^{2L} \sum_{j=0}^{2L} w_{ij}^c (\mathcal{Y}_{i,k|t} - \hat{\mathbf{y}}_k^-) (\mathcal{Y}_{j,k|t} - \hat{\mathbf{y}}_k^-)^T \\ \mathbf{P}_{\mathbf{x}_k \mathbf{y}_k} &= \sum_{i=0}^{2L} \sum_{j=0}^{2L} w_{ij}^c (\mathcal{X}_{i,k|t}^x - \hat{\mathbf{x}}_k^-) (\mathcal{Y}_{j,k|t} - \hat{\mathbf{y}}_k^-)^T \\ \mathbf{K}_k &= \mathbf{P}_{\mathbf{x}_k \mathbf{y}_k} \mathbf{P}_{\mathbf{y}_k}^{-1} \\ \hat{\mathbf{x}}_k &= \hat{\mathbf{x}}_k^- + \mathbf{K}_k (\mathbf{y}_k - \hat{\mathbf{y}}_k^-) \\ \mathbf{P}_{\mathbf{x}_k} &= \mathbf{P}_{\mathbf{x}_k}^- - \mathbf{K}_k \mathbf{P}_{\mathbf{y}_k} \mathbf{K}_k^T\end{aligned}$$

- *Parameters:* $\mathbf{x}^a = [\mathbf{x}^T \quad \mathbf{v}^T \quad \mathbf{n}^T]^T$, $\mathcal{X}^a = [(\mathcal{X}^x)^T \quad (\mathcal{X}^v)^T \quad (\mathcal{X}^n)^T]^T$, ζ is scaling parameter that determines the spread of the sigma-points around the prior mean, L is the dimension of the augmented state, \mathbf{R}_v is the process-noise covariance, \mathbf{R}_n is the observation-noise covariance, and w_i^m and w_{ij}^c are the scalar weights.

The specific type of resulting SPKF is determined by the choice of sigma-point selection scheme (weights & scaling factors) as well as the specific method by which the propagated sigma-points are combined in order to calculate the posterior covariance matrices. In the Appendix we summarize two specific SPKF approaches, the *unscented Kalman filter* (UKF)¹¹ and the *central difference Kalman filter* (CDKF).² We also include the *square-root* implementations, which propagate (and update) directly the square-root of the state covariance matrix, thus avoiding the need to perform a direct matrix square-root operation at each time step.^{2,4} This provides increased computational efficiency as well as robust numerical stability. Other variations include efficient implementations when the noise is assumed additive (allowing fewer sigma-points to be used), or for special state-transition structures (as with pure parameter estimation).^{5,12} Note that the overall computational complexity of the SPKF is the same as that of the EKF.

B. SPKF Application Examples

We provide two examples to illustrate the performance benefits of the SPKF. The first example corresponds to noisy *time-series* estimation with neural networks^a, and the second example is an *inverted double pendulum* control system. Although we only present two examples here, the SPKF has already been successfully applied to numerous other application.^{5,12,15–24} In all cases, the superiority over the EKF has been well documented.

1. Noisy chaotic time-series estimation

In this example a SPKF is used to estimate an underlying clean time-series corrupted by additive Gaussian white noise. The time-series used is the Mackey-Glass-30 chaotic series^{25,26} that is described by the following continuous time differential equation

$$\frac{dx(t)}{dt} = -0.1x(t) + \frac{0.2x(t-3)}{1+x(t-3)^{10}}, \quad (23)$$

where t is the continuous time variable and $x(t)$ is the time-series amplitude at time t . For this experiment, we modeled the discrete time version of this time series as a nonlinear autoregression

$$x_k = f(x_{k-1}, x_{k-2}, \dots, x_{k-M}; \mathbf{w}) + v_k, \quad (24)$$

where the model f (parameterized by \mathbf{w}) was first approximated by training a feed-forward neural network on a sampled clean sequence generated by Equation 23. The residual error after convergence was taken to be the process noise variance, i.e., σ_v^2 . Next, white Gaussian noise was added to the clean Mackey-Glass series to generate a noisy time-series $y_k = x_k + n_k$. The corresponding state-space representation is given by

$$\mathbf{x}_{k+1} = \mathbf{f}(\mathbf{x}_k; \mathbf{w}) + \mathbf{B}v_k \quad (25)$$

$$y_k = \mathbf{C}\mathbf{x}_k + n_k \quad (26)$$

which can be expanded as

$$\begin{bmatrix} x_{k+1} \\ x_k \\ \vdots \\ x_{k-M+2} \end{bmatrix} = \begin{bmatrix} f(x_k, x_{k-1}, \dots, x_{k-M+1}; \mathbf{w}) \\ \begin{bmatrix} 1 & 0 & 0 & 0 \\ 0 & \ddots & 0 & \vdots \\ 0 & 0 & 1 & 0 \end{bmatrix} \begin{bmatrix} x_{k-1} \\ \vdots \\ x_{k-M+1} \end{bmatrix} \end{bmatrix} + \begin{bmatrix} 1 \\ 0 \\ \vdots \\ 0 \end{bmatrix} v_k \quad (27)$$

$$y_k = \begin{bmatrix} 1 & 0 & \dots & 0 \end{bmatrix} \begin{bmatrix} x_k & x_{k-1} & \dots & x_{k-M+1} \end{bmatrix}^T + n_k. \quad (28)$$

In the estimation problem, the noisy-time series y_k is the only observed input to either the EKF or SPKF algorithms (all utilize the known neural network model). Note that for time-series estimation, both the EKF and the SPKF are $\mathcal{O}(L^2)$ complexity. Figure 3 shows sub-segments of the estimates generated by both the EKF and the SPKF (the original noisy time-series has a 3dB SNR). The superior performance of the SPKF algorithms are clearly visible. Table 1 summarizes the mean MSE as well as its variance for a Monte-Carlo run of 200 randomly initialized experiments. For each run a different realization of both the process and

^aSee Haykin¹³ or Bishop¹⁴ for a thorough review of neural network theory.

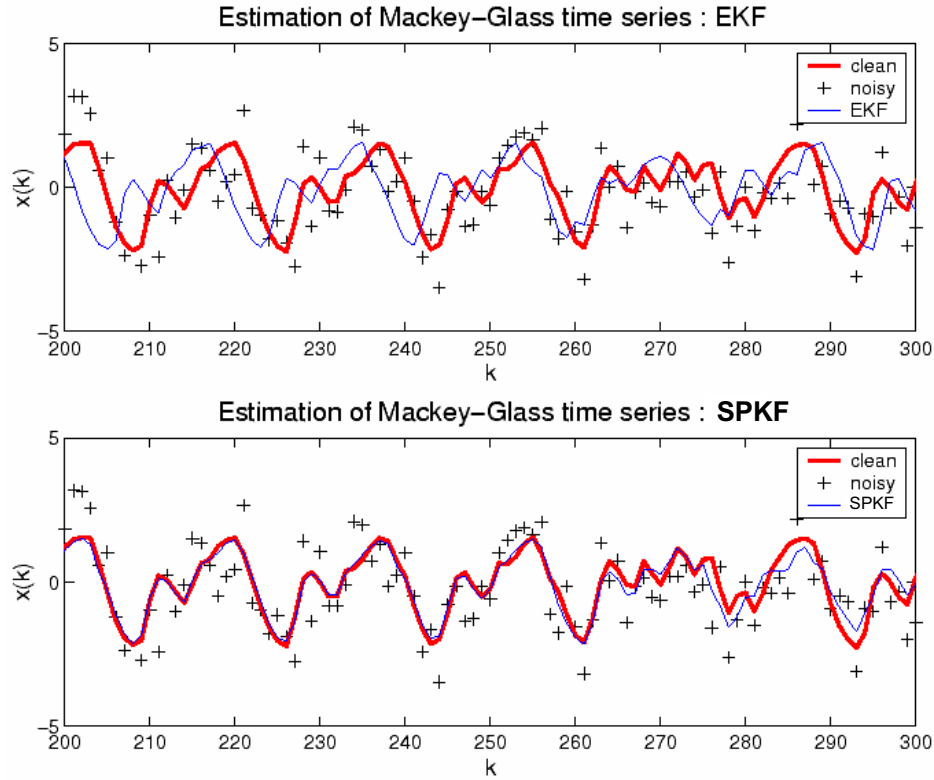


Figure 3. Estimation of Mackey-Glass time-series with the EKF and SPKF using a known model.

observation noise was generated. As is clearly evident from both the table and the figure, the magnitude of the EKF errors is much larger (close to 2 orders of magnitude) than those of the SPKFs. The EKF not only has a worse average MSE performance, but the variance of the MSE is also extremely large. This is due to the fact that every once in while (for some runs) the EKF completely diverges for a significant number of samples, resulting in huge spikes in the estimates and corresponding MSE.

Table 1. Estimation of Mackey-Glass time-series with the EKF and SPKF using a known model. : Monte-Carlo averaged (200 runs) estimation error.

Algorithm	MSE (mean)	MSE (var)
Extended Kalman filter (EKF)	60.90	4.475e8
Sigma-Point Kalman filter (SPKF)	0.1116	0.0341

2. Inverted Double Pendulum

An inverted double pendulum (See Figure 4) has states corresponding to cart position and velocity, and top and bottom pendulum angle and angular velocity; and system parameters correspond the length and mass of each pendulum, and the cart mass:

$$\mathbf{x} = \begin{bmatrix} x & \dot{x} & \theta_1 & \dot{\theta}_1 & \theta_2 & \dot{\theta}_2 \end{bmatrix}, \quad \mathbf{w} = \begin{bmatrix} l_1 & l_2 & m_1 & m_2 & M \end{bmatrix} \quad (29)$$

The continuous-time dynamics of the system (see Figure 4) are discretized with a sampling period of 0.02 seconds. The pendulum is stabilized by applying a control force, u to the cart. In this case we use a *state*

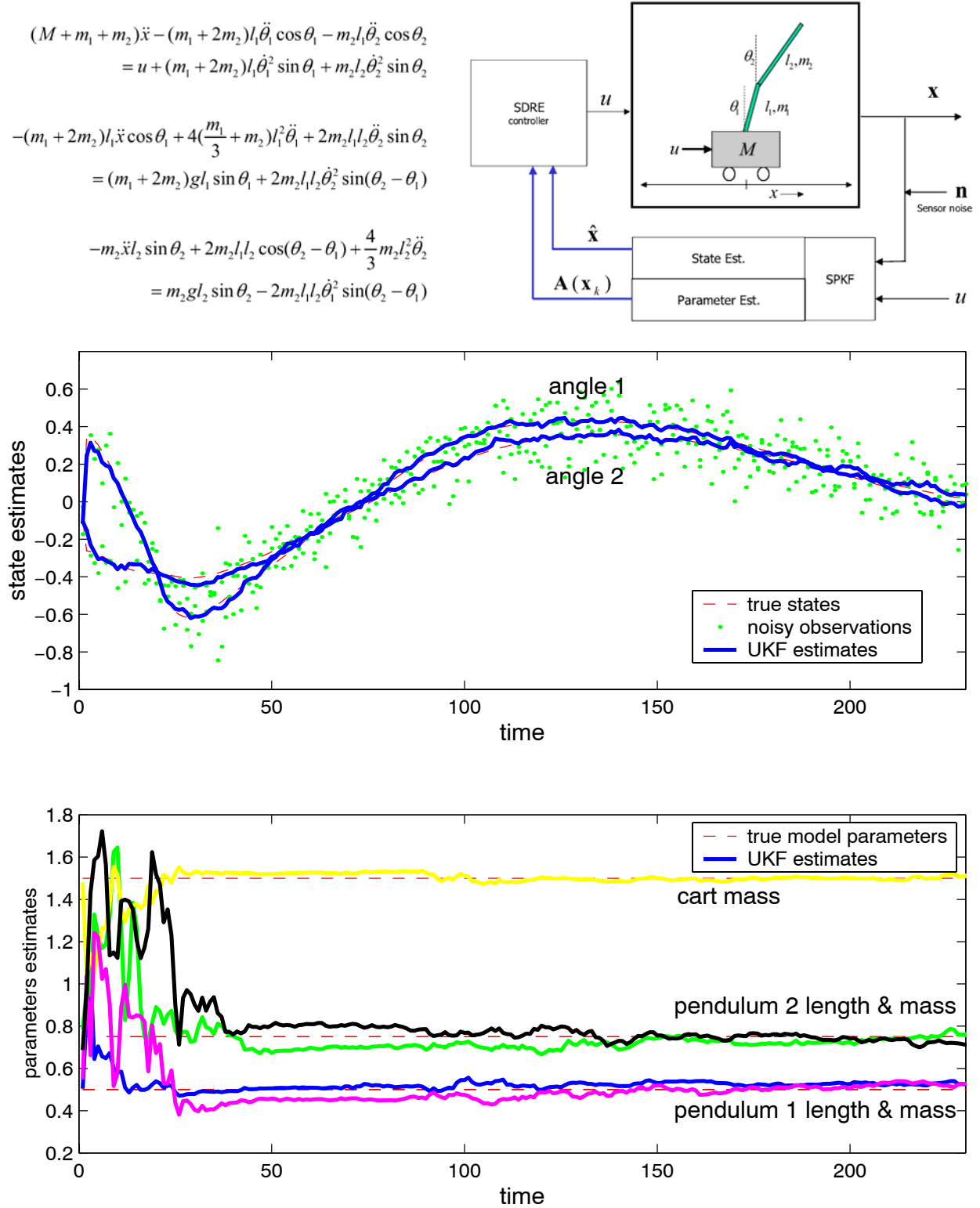


Figure 4. Inverted double pendulum dual estimation and control experiment. Dynamic model and schematic of control system (top plot). Estimation results are shown in the bottom plot: state estimates (top) and parameter estimates(bottom).

dependent Riccati equation (SDRE) controller to stabilize the system^b. The observation corresponds to noisy measurements of the cart position, cart velocity, and angle of the top pendulum. This is a challenging problem, as no measurements are made for the bottom pendulum, nor for the angular velocity of the top pendulum. For this experiment, the pendulum is initialized in a jack-knife position (+25/-25 degrees) with a cart offset of 0.5 meters. The SDRE controller needs accurate estimates of the system state as well as system parameters in order to accurately and robustly balance the pendulum. In our experiment, noisy observations of the system states were available and the system parameters were also initialized to incorrect values. A SPKF (a joint-UKF in this case) is used to estimate both the underlying system states and the true system parameters using only the noisy observations at each time step, which is then fed back to the SDRE controller for closed-loop control. Figure 4 illustrates the performance of this adaptive control system by showing the evolution of the estimated and actual states (middle) as well as the system parameter estimates (bottom). At the start of the simulation both the states and parameters are unknown (the control system is unstable at this point). However, within one trial, the SPKF enables convergence and stabilization of the pendulum without a single crash! This is in stark contrast to standard system identification and adaptive control approaches, where numerous off-line trials, large amounts of training data and painstaking “hand-tuning” are often needed. In this setup, the EKF is also able to balance the pendulum. However, the EKF is less robust. Often the EKF estimated parameters converge to wrong values, thus requiring better initial conditions and less noise on the observations.

IV. SPKF Based GPS/INS Integration

We now describe the application of the SPKF to the problem of loosely coupled GPS/INS integration for guidance, navigation and control (GNC) of an unmanned aerial vehicle (UAV). The main subcomponents of such a GNC system is a vehicle control system and a guidance & navigation system (GNS) as shown in Figure 5. Our UAV research platform (software simulator, hardware-in-the-loop simulator & flight vehicle) is based on a fully instrumented XCell-90 R/C helicopter (see Figure 5), originally designed by MIT’s *Laboratory for Information and Decision Systems*.²⁸ The avionics package includes an Inertial Sciences ISIS MEMS based IMU, an Ashtech G12 10Hz GPS, a barometric altimeter and a DSP Design TP400 PC104 based flight computer running QNX-4. Our nonlinear control system (which requires state-estimates) is based on an efficient *state-dependent Riccati-equation* (SDRE) framework that has proven to be significantly superior and more robust than standard LQR methods.^{29,30}

The existing GPS/INS navigation filter was based on an MIT designed high-performance hand-tuned EKF implementation.³¹ Our proposed estimator simply replaced the EKF in MIT’s system with a SPKF based estimator (SRCDKF). All our experimental results in later sections will use the original EKF based navigation filter as a baseline reference. As a further extension, we also implemented a SPKF based sensor latency compensation technique. We compared our SPKF based system performance to the baseline system with specific focus on: 1) Improved six-degrees-of-freedom (6DOF) state estimation accuracy, 2) SPKF based compensation for GPS latency, 3) Evaluation of improved closed-loop control envelope, and 4) Robustness to GPS outages. We will next discuss the UAV specific system process and observation (measurement) models used inside our SPKF (and EKF) based system.

A. Process Model

Even though we used a high-fidelity (70 parameters, 43 states) nonlinear dynamic model of UAV movement²⁹ for our UAV simulators and control system design, due to its high computational complexity it is not ideally suited for use within the navigation filter loop. For this reason we opted for the standard IMU driven kinematic process model formulation that comprises an INS mechanization component^{32,33} and a IMU sensor error model component. Because low cost MEMS based IMUs such as the one used in our avionics system have large bias and scale factor errors we included these components into our state vector to be estimated.

^bAn SDRE controller²⁷ is designed by formulating the dynamic equations as $\mathbf{x}_{k+1} = \mathbf{A}(\mathbf{x}_k)\mathbf{x}_k + \mathbf{B}(\mathbf{x}_k)\mathbf{u}_k$. Note, this representation is *not* a linearization, but rather a reformulation of the nonlinear dynamics into a pseudo-linear form. Based on this state-space representation, we design an optimal LQR controller, $\mathbf{u}_k = -\mathbf{R}^{-1}\mathbf{B}^T(\mathbf{x}_k)\mathbf{P}(\mathbf{x}_k)\mathbf{x}_k \equiv \mathbf{K}(\mathbf{x}_k)\mathbf{x}_k$, where $\mathbf{P}(\mathbf{x}_k)$ is a solution of the standard Riccati equations using state-dependent matrices $\mathbf{A}(\mathbf{x}_k)$ and $\mathbf{B}(\mathbf{x}_k)$. The procedure is repeated at every time step at the current state \mathbf{x}_k and provides local asymptotic stability of the plant.²⁷ The approach has been found to be far more robust than LQR controllers based on standard linearization techniques, and as well as many alternative “advanced” nonlinear control approaches.

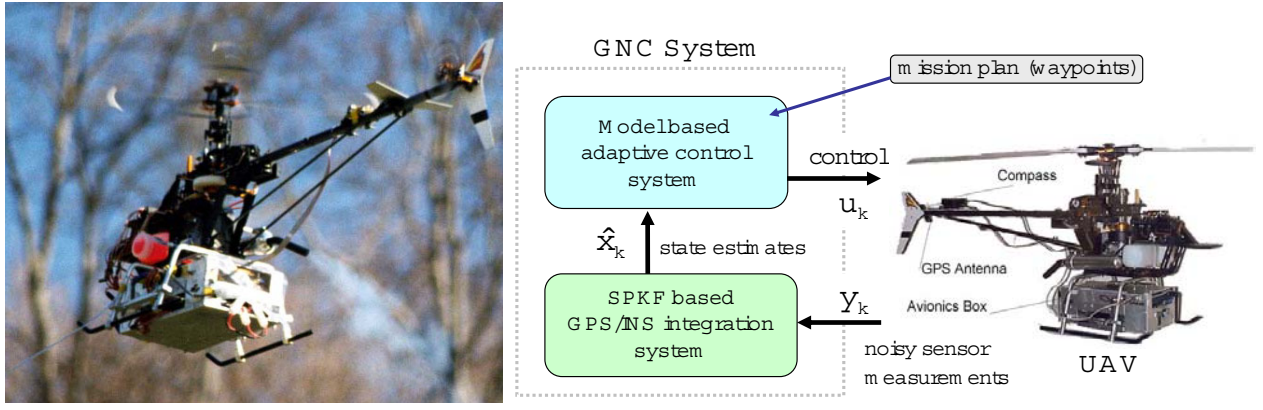


Figure 5. (left) Instrumented X-Cell-90 helicopter in flight. (right) Schematic diagram of unmanned aerial vehicle (UAV) guidance, navigation and control (GNC) system.

The estimated values of these error components are then used to correct the raw IMU acceleration and gyro-rate measurements before they are used inside the INS mechanization equations of the process model. The 16 dimensional state vector of our system is given by,

$$\mathbf{x} = \begin{bmatrix} \mathbf{p}^T & \mathbf{v}^T & \mathbf{e}^T & \mathbf{a}_b^T & \boldsymbol{\omega}_b^T \end{bmatrix} \quad (30)$$

where $\mathbf{p} = [x \ y \ z]^T$ and $\mathbf{v} = [v_x \ v_y \ v_z]^T$ are the position and velocity vectors of the vehicle in the navigation frame, $\mathbf{e} = [e_0 \ e_1 \ e_2 \ e_3]^T$ is the unity norm vehicle attitude quaternion, $\mathbf{a}_b = [a_{x_b} \ a_{y_b} \ a_{z_b}]^T$ is the vector of IMU acceleration biases, and $\boldsymbol{\omega}_b = [p_b \ q_b \ r_b]^T$ is the IMU gyro rate bias vector. Note that we could have include a separate *scale* factor in addition to the *bias* term in the state vector. However, in our experiments, we found it sufficient to model the combined effect of the bias and scale error terms as a single *time-varying* bias term.

The continuous time *kinematic* navigation equations (INS mechanization equations and error model) operating on this state vector and driven by the error corrected IMU measurements are given below:

$$\dot{\mathbf{p}} = \mathbf{v} \quad (31)$$

$$\dot{\mathbf{v}} = \mathbf{C}_b^n (\bar{\mathbf{a}} - \mathbf{a}_{r_{imu}}) + \begin{bmatrix} 0 & 0 & 1 \end{bmatrix}^T g \quad (32)$$

$$\dot{\mathbf{e}} = -\frac{1}{2} \tilde{\boldsymbol{\Omega}} \bar{\boldsymbol{\omega}} \mathbf{e} \quad (33)$$

$$\dot{\mathbf{a}}_b = \mathbf{w}_{\mathbf{a}_{b_k}} \quad (34)$$

$$\dot{\boldsymbol{\omega}}_b = \mathbf{w}_{\boldsymbol{\omega}_{b_k}} \quad (35)$$

\mathbf{C}_b^n is the direction cosine matrix (DCM) transforming vectors from the body frame to the navigation frame. The DCM is a nonlinear function of the current attitude quaternion and is given by

$$\mathbf{C}_b^n = (\mathbf{C}_n^b)^T = 2 \begin{bmatrix} 0.5 - e_2^2 - e_3^2 & e_1 e_2 - e_0 e_3 & e_1 e_3 + e_0 e_2 \\ e_1 e_2 + e_0 e_3 & 0.5 - e_1^2 - e_3^2 & e_2 e_3 - e_0 e_1 \\ e_1 e_3 - e_0 e_2 & e_2 e_3 + e_0 e_1 & 0.5 - e_1^2 - e_2^2 \end{bmatrix}. \quad (36)$$

The term g is the gravitational acceleration component and $\bar{\mathbf{a}}$ and $\bar{\boldsymbol{\omega}}$ are the bias and noise corrected IMU accelerometer and gyro rate measurements, i.e.,

$$\bar{\mathbf{a}} = \tilde{\mathbf{a}} - \mathbf{a}_b - \mathbf{n}_a \quad (37)$$

$$\bar{\boldsymbol{\omega}} = \tilde{\boldsymbol{\omega}} - \boldsymbol{\omega}_b - \mathbf{C}_n^b \boldsymbol{\omega}_c - \mathbf{n}_\omega. \quad (38)$$

In the above equations $\tilde{\mathbf{a}}$ and $\tilde{\boldsymbol{\omega}}$ are the raw measurements coming from the IMU, \mathbf{n}_a and \mathbf{n}_ω are the IMU acceleration and gyro-rate measurement noise terms, and $\boldsymbol{\omega}_c$ is the rotational rate of the earth as measured

in the navigation frame (Coriolis effect). In general, ω_c is a function of the location of the navigational frame relative to the earth frame and hence is time-varying as the navigation frame moves relative to the earth frame. However, for our purposes (aggressive autonomous UAV flight within a very small airspace volume) we assumed the navigation frame does not change relative to the earth frame resulting in a constant ω_c for a given origin location (lat/long) of our navigation frame. $\tilde{\Omega}_{\bar{\omega}}$ is a 4×4 skew-symmetric matrix³⁴ composed of the error corrected IMU gyro-rate measurements, i.e.,

$$\tilde{\Omega}_{\bar{\omega}} = \begin{bmatrix} 0 & \bar{\omega}_p & \bar{\omega}_q & \bar{\omega}_r \\ -\bar{\omega}_p & 0 & -\bar{\omega}_r & \bar{\omega}_q \\ -\bar{\omega}_q & \bar{\omega}_r & 0 & -\bar{\omega}_p \\ -\bar{\omega}_r & -\bar{\omega}_q & \bar{\omega}_p & 0 \end{bmatrix}. \quad (39)$$

In Eq. (32), $\mathbf{a}_{\mathbf{r}_{imu}}$ is the IMU-lever-arm coupling component due to the IMU not being located at the center of gravity of the vehicle. This component can be ignored if the navigation filter computes the state estimate at the IMU location. This IMU centric navigation solution can then simply be transformed to the center of gravity location after the fact as needed by the vehicle control system.

The final components of the process model, Eqs. (34) and (35) models the time-varying nature of the IMU sensor bias error terms. Usually, sensor error in an INS are modelled as a zero-mean, stationary, first-order Gauss-Markov process.³⁵ Since the biases and scale factors of low cost MEMS based IMU sensors exhibit non-zero mean and non-stationary behaviour, the errors are modelled as a *random walk*, in order to improve the tracking of these time-varying errors by the navigation filter. This does however require that the effect of these errors be *observable* through the specific choice of measurement model.

The position and velocity discrete-time updates are calculated by the following simple first-order Euler update

$$\mathbf{p}_{k+1} = \mathbf{p}_k + \dot{\mathbf{p}}_k \cdot dt \quad (40)$$

$$\mathbf{v}_{k+1} = \mathbf{v}_k + \dot{\mathbf{v}}_k \cdot dt, \quad (41)$$

where $\dot{\mathbf{p}}_k$ and $\dot{\mathbf{v}}_k$ are calculated using Eqs. (31) and (32) and dt is the integration time-step of the system (in our system this was dictated by the IMU rate, i.e., $dt = 10ms$). The quaternion propagation equation can be discretized with an analytical calculation of the exponent of the skew-symmetric matrix given by Stevens.³⁴ The discrete-time update can be written as

$$\mathbf{e}_{k+1} = \exp\left(-\frac{1}{2}\tilde{\Omega} \cdot dt\right) \mathbf{e}_k. \quad (42)$$

If we further denote

$$\Delta\phi = \bar{\omega}_p \cdot dt \quad (43)$$

$$\Delta\theta = \bar{\omega}_q \cdot dt \quad (44)$$

$$\Delta\psi = \bar{\omega}_r \cdot dt, \quad (45)$$

as effective rotations around the (body frame) roll, pitch and yaw axes undergone by the vehicle during the time period dt , assuming that the angular rates $\bar{\omega}_p, \bar{\omega}_q$ and $\bar{\omega}_r$ remained constant during that interval, we can introduce the 4×4 skew-symmetric matrix

$$\Phi_{\Delta} = \tilde{\Omega} \cdot dt = \begin{bmatrix} 0 & \Delta\phi & \Delta\theta & \Delta\psi \\ -\Delta\phi & 0 & -\Delta\psi & \Delta\theta \\ -\Delta\theta & \Delta\psi & 0 & -\Delta\phi \\ -\Delta\psi & -\Delta\theta & \Delta\phi & 0 \end{bmatrix}. \quad (46)$$

Using the definition of the matrix exponent and the skew symmetric property of Φ_{Δ} , we can write down the following closed-form solution:

$$\exp\left(-\frac{1}{2}\Phi_{\Delta}\right) = \mathbf{I} \cos(s) - \frac{1}{2}\Phi_{\Delta} \frac{\sin(s)}{s}, \quad (47)$$

where

$$s = \frac{1}{2} \left\| \begin{bmatrix} \Delta\phi & \Delta\theta & \Delta\psi \end{bmatrix} \right\| = \frac{1}{2} \sqrt{(\Delta\phi)^2 + (\Delta\theta)^2 + (\Delta\psi)^2} . \quad (48)$$

See Gavrillets³¹ and Van der Merwe⁵ for proofs of this closed-form solution. Eqs. (42) and (47) ensure (at least theoretically) that the updated quaternion \mathbf{e}_{k+1} has a unit norm. However, a small Lagrange multiplier term can be added to the first component of Equation 47 to further maintain numerical stability and the unity norm of the resulting quaternion. The resulting final solution for the time-update of the quaternion vector is given by

$$\mathbf{e}_{k+1} = \left[\mathbf{I}(\cos(s) + \eta \cdot dt \cdot \lambda) - \frac{1}{2} \mathbf{\Phi}_\Delta \frac{\sin(s)}{s} \right] \mathbf{e}_k . \quad (49)$$

where $\lambda = 1 - \|\mathbf{e}_k\|^2$ is the deviation of the square of the quaternion norm from unity due to numerical integration errors, and η is the factor that determines the convergence speed of the numerical error. These factors serve the role of the above mentioned Lagrange multiplier that ensures that the norm of the quaternion remains close to unity.³⁶ The constraint on the speed of convergence for stability of the numerical solution is $\eta \cdot dt < 1$.³¹

Finally, the discrete time random-walk process for the IMU sensor error terms are given by

$$\mathbf{a}_{b_{k+1}} = \mathbf{a}_{b_k} + dt \cdot \mathbf{w}_{\mathbf{a}_{b_k}} \quad (50)$$

$$\boldsymbol{\omega}_{b_{k+1}} = \boldsymbol{\omega}_{b_k} + dt \cdot \mathbf{w}_{\boldsymbol{\omega}_{b_k}} , \quad (51)$$

where $\mathbf{w}_{\mathbf{a}_{b_k}}$ and $\mathbf{w}_{\boldsymbol{\omega}_{b_k}}$ are zero-mean Gaussian random variables.

Note that these navigation equations are considered a *direct* formulation, as opposed to the alternative *indirect* (error) formulation. This choice was made for consistency with the MIT EKF implementation. The trade-offs between direct versus indirect formulations with the SPKF are currently being investigated.

B. Observation Models

Our system made use of 2 independent avionic sensors to aid the INS: a 10Hz, 50ms latency GPS (Ashtech G12) and a barometric altimeter that measures absolute altitude as a function of ambient air pressure. The observation models used in our system for these sensors (see below) are highly nonlinear, making the use of the SPKF framework again preferable to an EKF solution.

GPS: Since our GPS antenna is not located at the same location in the body frame as the IMU, it not only observes the bodies position and velocity in the navigation frame, but also the body's attitude relative to the navigation frame due to the "lever-arm effect". More specifically, the GPS observation model is given by:

$$\mathbf{p}_k^{GPS} = \mathbf{p}_{k-N} + \mathbf{C}_b^n \tilde{\mathbf{r}}_{gps} + \mathbf{n}_{p_k} \quad (52)$$

$$\mathbf{v}_k^{GPS} = \mathbf{v}_{k-N} + \mathbf{C}_b^n \boldsymbol{\omega}_{k-N} \times \tilde{\mathbf{r}}_{gps} + \mathbf{n}_{v_k} , \quad (53)$$

where \mathbf{p}_{k-N} and \mathbf{v}_{k-N} are the time-delayed (by N samples due to sensor latency) 3D navigation-frame position and velocity vectors of the vehicle, $\tilde{\mathbf{r}}_{gps}$ is the location of the GPS antenna in the body frame (relative to the IMU location), $\boldsymbol{\omega}_{k-N}$ are the true rotational rates of the vehicle at time $k - N$, and \mathbf{n}_{p_k} and \mathbf{n}_{v_k} are stochastic measurement noise terms. Here the noise terms are modeled as being time-dependent. This is due to the fact that the accuracy of observations vary over time according to the current PDOP value of the loosely coupled GPS solution. Since the DCM, \mathbf{C}_b^n , in Eqs. (52) and (53) are a function of the attitude quaternion, the GPS measurements provides information not only of the vehicles position and velocity, but also of its attitude. This removes the need for an absolute attitude sensor such as a magnetic compass or tilt-sensor. However, this will also result in the non-observability of the IMU sensor errors during prolonged periods of GPS outages, which in turn can lead to significant INS drift.

The time delay (N samples) in the GPS model equations is due to the internal GPS processing latency inherent to all loosely coupled GPS solutions. This implies that the latest GPS measurement relates to the state of the vehicle as it was a number of samples in the past. If the specific latency of the GPS is small, it can (and often is) ignored. However, if the latency is significant, care must be taken when fusing this lagged information with the current estimate of the vehicle's state in the measurement update step of the Kalman filter.

Barometric altimeter: Ambient air pressure provides an accurate source of sea-level altitude information. Important sources of error are sensor quantization and measurement noise. We used a high-end altimeter with $10^{-3}psi$ (0.6 meters) resolution. The measurement noise was assumed to be zero-mean, white and Gaussian. The observation model that incorporates these effects are:

$$z_k^{alt} = -\frac{1}{\varphi} \ln \left[\frac{\rho_0^q \lfloor (\rho_0 \exp(\varphi \cdot z_k) + n_{z_a}) / \rho_0^q \rfloor}{\rho_0} \right] \quad (54)$$

where ρ_0 is the nominal air pressure at sea-level, φ is the pressure decay rate with altitude constant ($1.16603 \times 10^{-4}psi/m$), z_k is the current navigation-frame z-axis position of the vehicle, ρ_0^q is the air pressure quantization resolution of the altimeter ($10^{-3}psi$), z_k^{alt} is the altimeter output and $\lfloor \cdot \rfloor$ is the integer flooring function. This model is not only a nonlinear function of the state, but the measurement noise also effects the output altitude measurement in a non-additive fashion. Again, for such a model the use of the SPKF not only allows for a much simpler implementation than the EKF (no analytical derivatives need to be calculated), but will also results in more accurate estimation results.

C. SPKF Based Sensor Latency Compensation

One of the big challenges in building a robust state estimator for loosely coupled GPS/INS systems is dealing with the inherent measurement latency of the GPS sensor. As mentioned in the previous section, a GPS sensors has a finite processing delay between when the GPS satellite signals are received for processing and when the actual position and velocity measurement related to those signals becomes available. This implies that the current GPS reading actually corresponds to the position and velocity state of the vehicle at some point in the past. This time difference is called the measurement latency. For cheaper lower performance GPS systems this latency can be several seconds, causing serious problems when these measurements are fused (inside a Kalman filter) with the current prediction of the vehicle state. Short if *ignoring* the latency issue completely, previous approaches either store all of the state estimates and observations during the latency period and then *re-run* the complete filter when the latency lagged observation finally arrives, or apply accumulated correction terms to the state estimate based on a time-convolved linearized approximation of the system.⁹ The first approach, although accurate incurs an exceedingly high computational penalty, precluding its use in real-time systems. The second approach on the other hand can be highly inaccurate if the system process and measurement equations are significantly nonlinear.

For our SPKF based navigation filter, we derived a new approach to deal with the latency issue based on accurately maintaining the relevant *cross-covariance matrices across time*. These terms are needed to formulate a modified Kalman gain matrix, which is used to fuse the current prediction of the state with an observation related to a prior (lagged) state of the system. The system process model is first augmented such that a copy of the prior system state is maintained across time. The observation model is also adapted to relate the current GPS observation to this *lagged* (but-maintained) state. The correct gain terms are then automatically calculated inside the SPKF filter. The SPKF allows for such a simple solution due to the fact that it does not need to linearize the system equations when calculating the relevant posterior statistics. For a more detailed exposition of this method, see Appendix B.

V. Experimental Results

This section presents a number of experimental results comparing our proposed SPKF based GPS/INS system with a similar system built around an EKF implementation. The first set of experiments were all performed in simulation using the high-fidelity MIT-Draper-XCell-90 model based UAV simulator platform.³¹ All relevant avionic sensors (IMU, GPS, altimeter, etc.) as well as all actuators were accurately modeled, including effects such as GPS latency and IMU sensor bias errors and drift. The purpose of the simulation based experiments is to compare the performance of our new proposed SPKF approaches to that of the existing EKF approach in a controlled (repeatable) environment where the *ground truth* state information is available. This allows for objective comparison of estimation accuracy.

The second set of experiments were performed on real flight data using telemetry recordings of actual autonomous flights performed by the UAV. Although ground truth information is not available for these experiments to judge absolute accurate, it still allows for direct qualitative comparison between the EKF and SPKF based systems. Specific performance issues related to real world events such as GPS outages were investigated.

A. Simulation Experiments

The first simulated experiment performed was used to provide quantitative comparisons between the EKF, SPKF, and latency compensated SPKF. The helicopter was flown (in simulation) along a complex trajectory that increased in “aggressiveness” over time. Figure 6 shows a 3D representation of this flight-plan trajectory with the helicopter’s true attitude superimposed at certain intervals. The simulated flight included complex acrobatic maneuvers such as *rapid-rise-and-hover*, *figure-eights*, *split-s*, etc. For this experiment we did not “close the loop” for the flight control system. In other words, the control system used the true known states of vehicle for the online calculation of the control law. The SPKF or EKF estimated state was not fed back to the control system. This was done to ensure that the helicopter flew exactly the same flight profile when comparing the performance of the different estimators.

Table 2 compares the average root-mean-square (RMS) estimation errors for the three different state estimators. We also show (in brackets) the relative error reduction percentage for each of the two SPKF estimators compared to the EKF. The normal SPKF is able to reduce the 3D position and velocity estimation errors by about 10% and the roll and pitch angle estimation errors by about 20%.

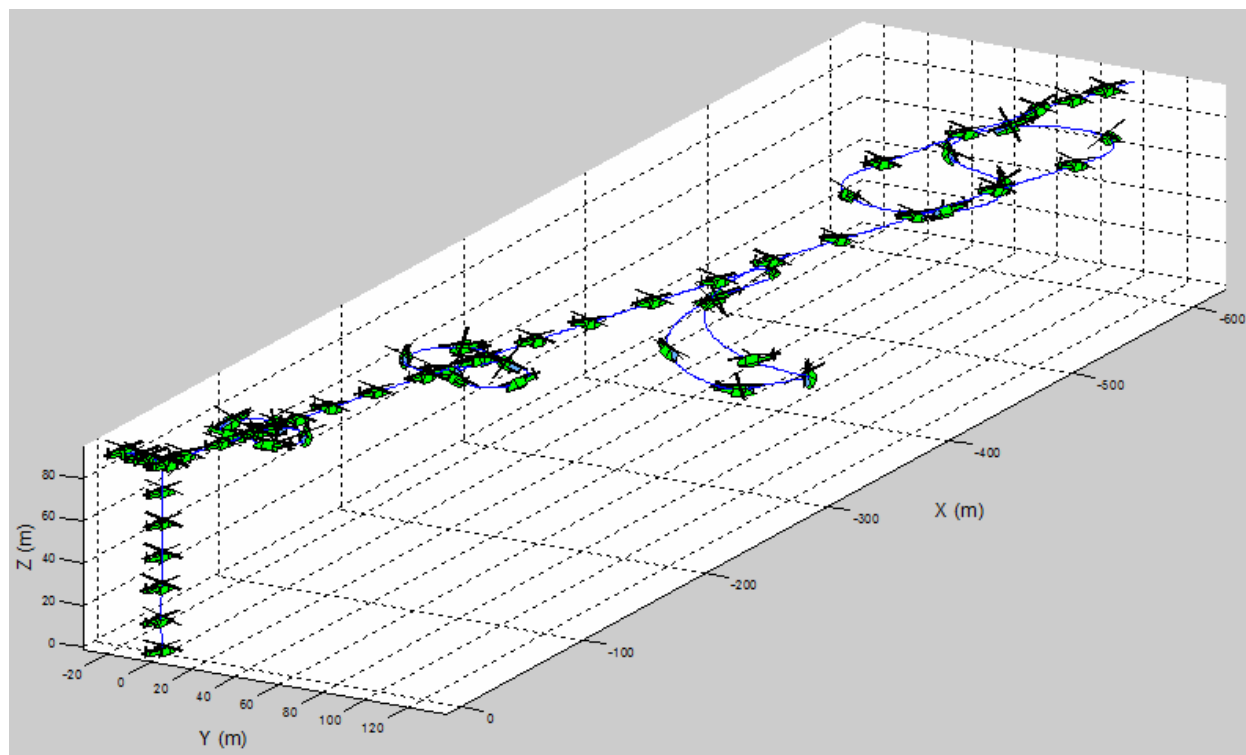


Figure 6. Simulated UAV trajectory used for state estimation experiments.

The biggest improvement over the EKF, 55%, is in the estimation of the yaw (heading) angle. The GPS latency compensated SPKF goes even further with a 33% reduction in position, velocity, roll angle and pitch angle errors. The yaw angle error reduction is again the highest at 65%. We repeated this experiment numerous times with different initializations and realizations of measurement noise as well as flying different flight trajectories and all of the results consistently confirmed the same relative performance between the different estimators as presented in this experiment. Clearly, even though the normal SPKF already outperforms the EKF (as expected), correctly accounting for GPS latency is well worth the extra effort. The position and velocity estimation errors are shown in the top two plots of Figure 7 and the Euler angle estimation errors are shown in the bottom three plots. As before the SPKF clearly outperforms the EKF with the largest improvement again evident in the yaw (heading) angle estimation error. Figure 7 indicates how the EKF has a very large error in the yaw estimate for the first 80 seconds of the flight. This is due to a significant initial error in the underlying IMU bias error estimates. Even though the EKF and

SPKF filters were initialized with exactly the same initial state estimates^c, the SPKF was able to converge to the true biases in the IMU measurements much quicker and then track them more accurately. This

Table 2. UAV state estimation results : EKF vs. SPKF (with and without GPS latency compensation). The table reports average (over complete flight trajectory) root-mean-square (RMS) estimation errors for the EKF, SPKF (without GPS latency compensation) and SPKF (with GPS latency compensation) for the simulated flight shown in Figure 6. The estimation error reduction percentages are shown for all filters (relative to EKF).

Algorithm	Average RMS Error				
	position	velocity	Euler angles (degrees)		
	(m)	(m/s)	roll	pitch	yaw
EKF	2.1	0.57	0.25	0.32	2.29
SPKF (without latency compensation)	1.9 (10%)	0.52 (9%)	0.20 (20%)	0.26 (19%)	1.03 (55%)
SPKF (with latency compensation)	1.4 (32%)	0.38 (34%)	0.17 (32%)	0.21 (34%)	0.80 (65%)

result has been corroborated independently in Shin²⁴ (experiments focused on in-flight IMU *alignment*). This contributes (among other things) to more accurate Euler angle estimates. Although the average yaw estimate error improvement for the SPKF over the whole trajectory is 65%, this value does not accurately reflect the expected steady-state (after bias convergence) performance of the SPKF. Discounting this period, the average error improvement after bias convergence ($t > 80$ s) is 43%. The steady-state error improvement of the SPKF over the EKF is thus 32%, 34% and 43% respectively for the roll, pitch and yaw angle estimates.

Another interesting performance characteristic to note from the Euler angle estimates in Figure 7 are the frequent high peaks in the EKF’s estimation error plots. These coincide with the onsets of aggressive maneuvers (banking, turns, rapid climbs, etc.) that pushes the vehicle into regimes of increased nonlinear response. The linearization errors of the EKF will therefore be more severe at these times resulting in poor estimation performance and increase estimation error. In contrast the SPKF is able to deal with these increased nonlinearities quite satisfactorily.

In the second set of simulated experiments we “closed the loop” in the GNC system by feeding the estimated states back to the SDRE control system. In other words, the vehicle control commands will now be a function of the estimates generated by either the EKF or SPKF estimator and not of the “true” vehicle states. This mimics (in simulation) the true interdependency between the estimation and control system as would occur in the real flight hardware during a fully autonomous flight. The helicopter is commanded to perform an aggressive high speed nose-in turn. This maneuver requires the helicopter to fly along an imaginary circular trajectory while constantly pointing its nose towards the exact center of the circle. Accurate position, velocity and especially yaw angle estimates are needed to follow the desired flight plan with the desired attitude. Figure 8 shows the results of this experiment for both the EKF and SPKF. The desired flight trajectory is indicated by the red curve, the true realized trajectory in blue and the estimated trajectory in green. The true attitude of the helicopter is indicated by periodic renderings of the vehicle itself along the flight path. Clearly for the SPKF case the estimated trajectory is not only close to the true trajectory (small estimation error), but the true trajectory is close to the *desired* trajectory which indicated good control performance. The EKF plots clearly shows worse performance according to both these criteria. Also evident from the plots is the much improved yaw angle tracking performance of the SPKF system compared to the EKF system. The helicopter renderings for the EKF indicate that the nose is not consistently pointing at the true center of the desired circle. The SPKF system, on the other hand, does much better in estimating and realizing the correct yaw attitude for this maneuver.

B. Real Flight Data Experiments

Figure 9 shows the estimation results of the SPKF compared to the EKF based system on real flight telemetry. The UAV was flown under pilot guidance to a specified altitude at which point the system was switched

^cNote, while Figure 7 seems to indicate that there is a difference in the initial conditions for the yaw estimates of the two filters, this is actually due to a jump in the estimates after the first time step.

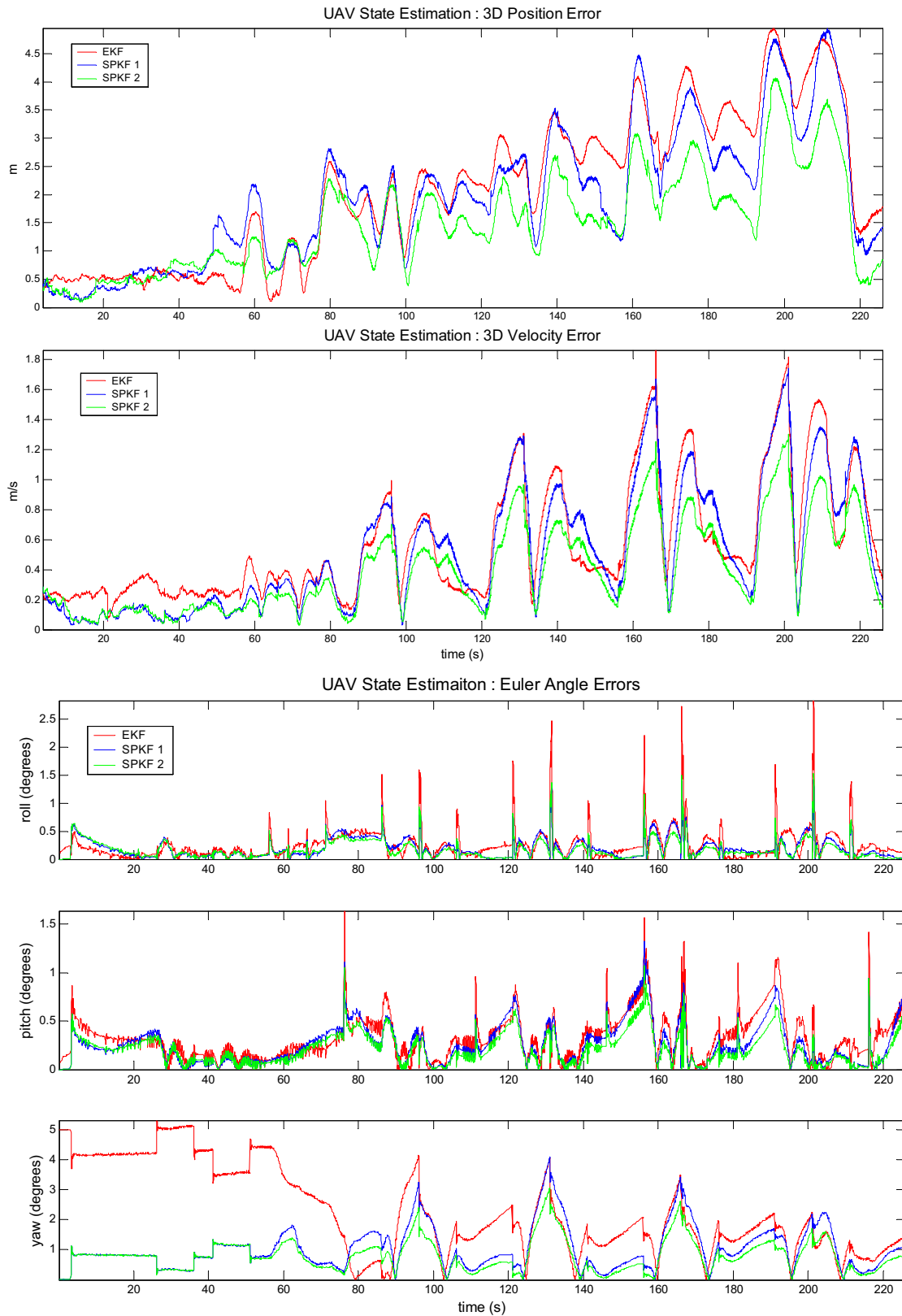


Figure 7. State estimation results: EKF vs. SPKF (*without* GPS latency compensation: SPKF 1) vs. SPKF (*with* GPS latency compensation: SPKF 2).

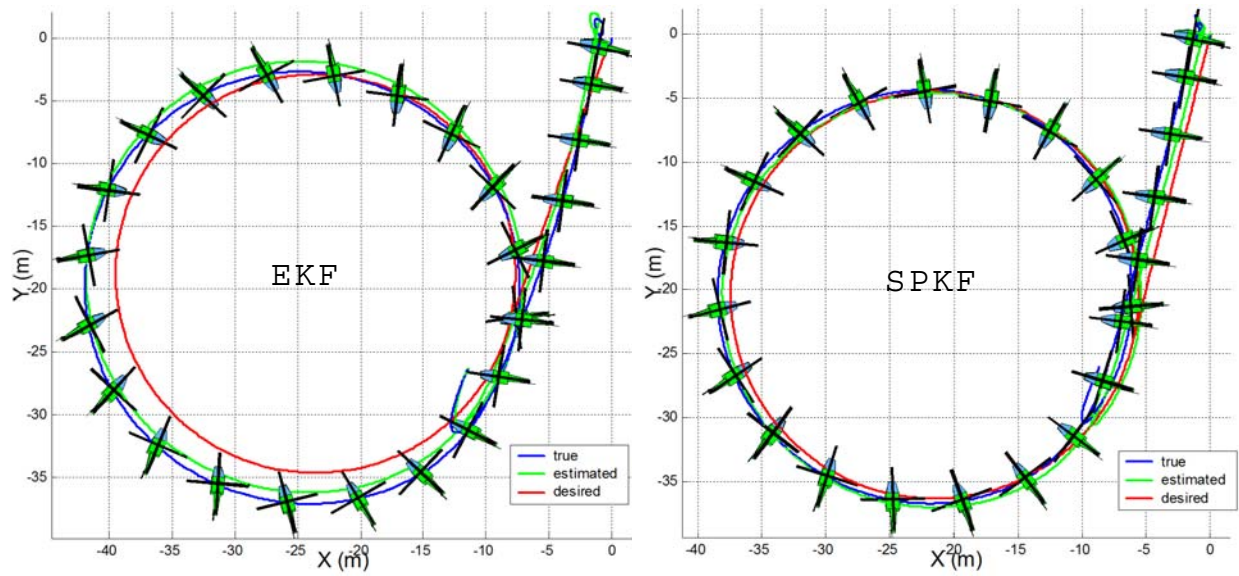


Figure 8. Closed-loop control performance comparison.

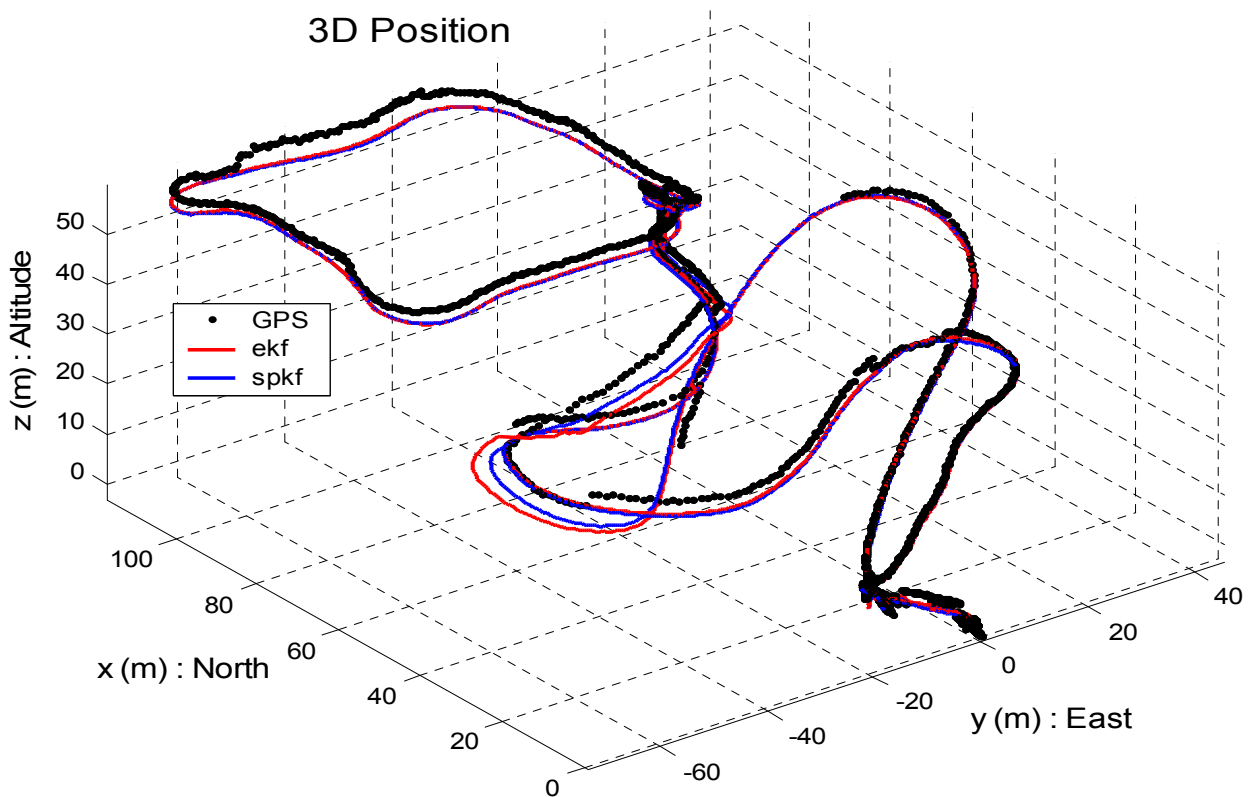


Figure 9. Estimated 3D position of test flight. The UAV lifted off and flew a complex sweeping S-maneuver until it reached its hover altitude at about 50m. At this point it hovered for a number of seconds after which it attempted to fly a horizontal square-profile. After the square was completed it hovered again for a number of seconds and then landed.

over to fully autonomous flight. The autonomous flight plan was as follows: First the UAV held steady in hover for a number of seconds, after which it flew a square trajectory at a constant altitude of about 55-60 meters. Since no ground truth signal is available for absolute error comparison, we need to evaluate the results on more subjective terms. For this purpose, a top-down (2D) projection of the estimation results is quite insightful (see Figure 10).

Notice the significant number of GPS outages that occurred during the pilot guided ascent to the hovering altitude (s-shaped curve). Clearly the SPKF appears to more accurately track the (assumed) true underlying trajectory during this outage period. The EKF generated position estimate exhibits an erratic jump just before the GPS measurements becomes available again (see Figure 10 at coordinates $\{40, -60\}$). This error is due to the inherent nature of the INS solution (derived from integrating the bias compensated IMU gyro and accelerometer data) to drift during periods of GPS outage. Since the SPKF performs a more accurate time-update during these periods than the EKF, and possibly also more accurately tracks the underlying IMU biases, the resulting SPKF estimates appear more robust to GPS outages in general. We are still investigating these claims further.

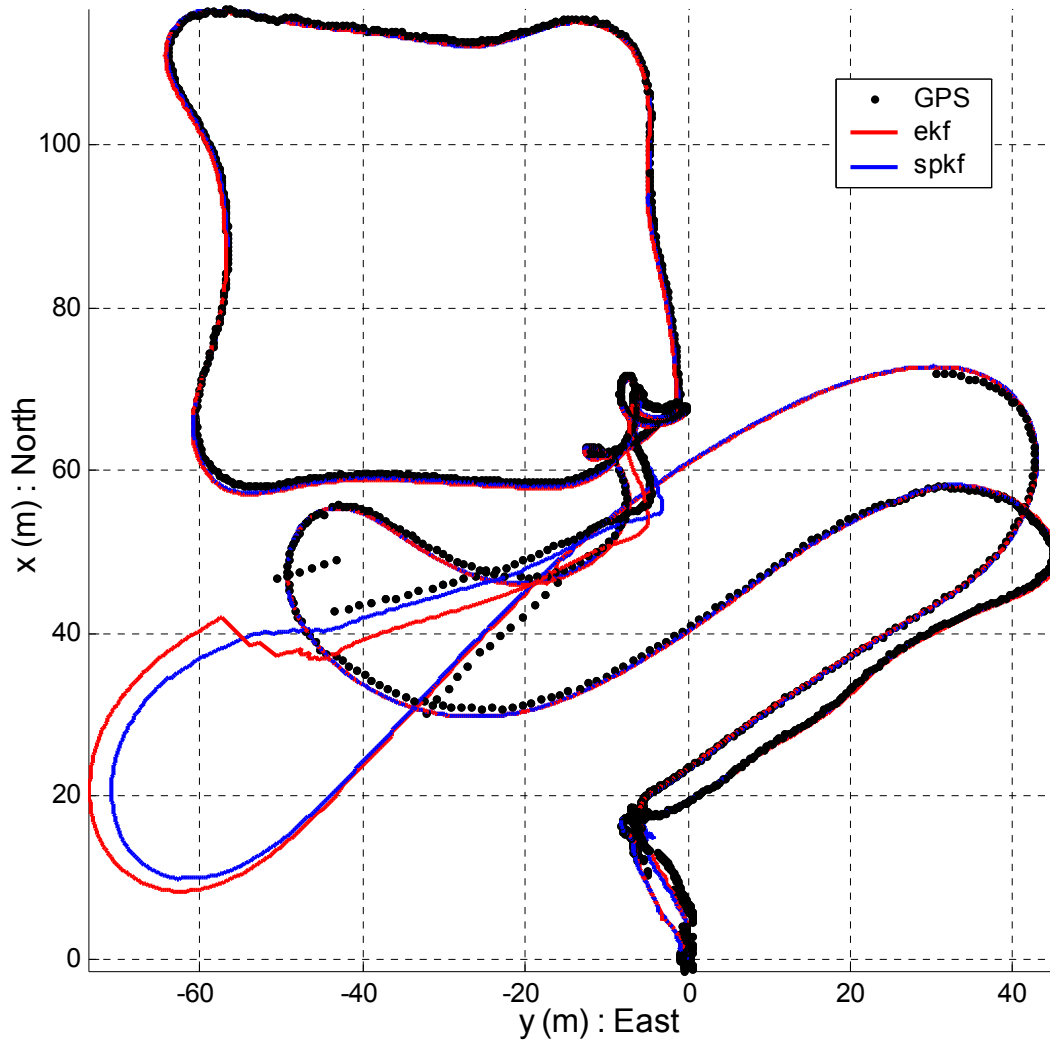


Figure 10. Estimated 2D position of test flight (top view)

VI. Conclusions

In this paper we provided a review of Sigma-Point Kalman filter methods for probabilistic inference. The SPKF provides superior performance over the current industry standard, EKF, by better accounting for nonlinearities and accommodating asynchronous and lagged sensor measurements. The computational complexity of the SPKF is equivalent to the EKF. Several examples were provided to illustrate the performance benefits. We then focused on the detailed design of an integrated navigation system. Relative to the EKF, the SPKF solution provided superior state estimation performance, better bias tracking, and improved robustness to GPS outages. While performance comparisons were based on a specific UAV rotor craft platform, the general implementation of the navigation filter and SPKF approach makes it applicable to general integrated navigation systems, with performance gains expected independent of the vehicle or specific sensors used.

We continue to investigate trade-offs between direct and indirect navigation equations, alternative quaternion representations, ability to track scale and bias, as well as robustness to GPS outages. Additional extensions include a tightly-coupled integration approach and additional sensor augmentations. We are also investigating the utility of replacing the higher-end IMU in our INS system with a low-cost IMU (<\$1000). Such IMUs typically have worse error performance (higher bias, scale-factor & drift), which can hopefully be compensated through the enhanced estimation performance of the SPKF based system.

Appendix A : SPKF Variant Pseudo-Code

This section provides the algorithmic pseudo-code for four different SPKF implementations. The first is based on the *unscented transformation* (a SPA scheme proposed by Julier & Uhlmann¹) and is called the *unscented Kalman filters* (UKF). The second SPKF is based on the *central-difference transformation* (a SPA scheme proposed separately by Norgaard et al.² and Ito et al.³⁷) and is called the *central difference Kalman filters* (CDKF). We also provide the pseudo-code for numerical robust and efficient *square-root* versions of these SPKFs. These algorithms, the *square-root UKF* (SR-UKF) and the *square-root CDKF* (SR-CDKF) was first published by Van der Merwe & Wan.^{3,4}

A. Unscented Kalman Filter (UKF)

- *Initialization:*

$$\begin{aligned}\hat{\mathbf{x}}_0 &= E[\mathbf{x}_0] \quad , \quad \mathbf{P}_{\mathbf{x}_0} = E[(\mathbf{x}_0 - \hat{\mathbf{x}}_0)(\mathbf{x}_0 - \hat{\mathbf{x}}_0)^T] \\ \hat{\mathbf{x}}_0^a &= E[\mathbf{x}_0^a] = \begin{bmatrix} \hat{\mathbf{x}}_0^T & \hat{\mathbf{v}}_0^T & \hat{\mathbf{n}}_0^T \end{bmatrix}^T \\ \mathbf{P}_0^a &= E[(\mathbf{x}_0^a - \hat{\mathbf{x}}_0^a)(\mathbf{x}_0^a - \hat{\mathbf{x}}_0^a)^T] \\ &= \begin{bmatrix} \mathbf{P}_{\mathbf{x}_0} & \mathbf{0} & \mathbf{0} \\ \mathbf{0} & \mathbf{R}_v & \mathbf{0} \\ \mathbf{0} & \mathbf{0} & \mathbf{R}_n \end{bmatrix}\end{aligned}$$

- For $k = 1, \dots, \infty$:

1. Set $t = k - 1$
2. Calculate sigma-points:

$$\mathcal{X}_t^a = \begin{bmatrix} \hat{\mathbf{x}}_t^a & \hat{\mathbf{x}}_t^a + \gamma\sqrt{\mathbf{P}_t^a} & \hat{\mathbf{x}}_t^a - \gamma\sqrt{\mathbf{P}_t^a} \end{bmatrix}$$

3. Time-update equations:

$$\begin{aligned}\mathcal{X}_{k|t}^x &= \mathbf{f}(\mathcal{X}_t^x, \mathcal{X}_t^v, \mathbf{u}_t) \\ \hat{\mathbf{x}}_k^- &= \sum_{i=0}^{2L} w_i^m \mathcal{X}_{i,k|t}^x \\ \mathbf{P}_{\mathbf{x}_k}^- &= \sum_{i=0}^{2L} w_i^c (\mathcal{X}_{i,k|t}^x - \hat{\mathbf{x}}_k^-) (\mathcal{X}_{i,k|t}^x - \hat{\mathbf{x}}_k^-)^T\end{aligned}$$

4. Measurement-update equations:

$$\begin{aligned}
\mathbf{y}_{k|t} &= \mathbf{h}(\mathbf{x}_{k|t}^x, \mathbf{x}_t^n) \\
\hat{\mathbf{y}}_k^- &= \sum_{i=0}^{2L} w_i^m \mathbf{y}_{i,k|t} \\
\mathbf{P}_{\hat{\mathbf{y}}_k} &= \sum_{i=0}^{2L} w_i^c (\mathbf{y}_{i,k|t} - \hat{\mathbf{y}}_k^-) (\mathbf{y}_{i,k|t} - \hat{\mathbf{y}}_k^-)^T \\
\mathbf{P}_{\mathbf{x}_k \mathbf{y}_k} &= \sum_{i=0}^{2L} w_i^c (\mathbf{x}_{i,k|t}^x - \hat{\mathbf{x}}_k^-) (\mathbf{y}_{i,k|t} - \hat{\mathbf{y}}_k^-)^T \\
\mathbf{K}_k &= \mathbf{P}_{\mathbf{x}_k \mathbf{y}_k} \mathbf{P}_{\hat{\mathbf{y}}_k}^{-1} \\
\hat{\mathbf{x}}_k &= \hat{\mathbf{x}}_k^- + \mathbf{K}_k (\mathbf{y}_k - \hat{\mathbf{y}}_k^-) \\
\mathbf{P}_{\mathbf{x}_k} &= \mathbf{P}_{\mathbf{x}_k}^- - \mathbf{K}_k \mathbf{P}_{\hat{\mathbf{y}}_k} \mathbf{K}_k^T
\end{aligned}$$

- *Parameters:* $\gamma = \sqrt{L + \lambda}$, $w_0^m = \lambda / (L + \lambda)$, $w_0^c = w_0^m + (1 - \alpha^2 + \beta)$, $w_i^c = w_i^m = 1 / [2(L + \lambda)]$ for $i = 1, \dots, 2L$. $\lambda = \alpha^2(L + \kappa) - L$ is a compound scaling parameter, L is the dimension of the augmented state-vector, $0 < \alpha \leq 1$ is the primary scaling factor determining the extent of the spread of the sigma-points around the prior mean. Typical range for α is $1e-3 < \alpha \leq 1$. β is a secondary scaling factor used to emphasize the weighting on the zeroth sigma-point for the posterior covariance calculation. β can be used to minimize certain higher-order error terms based on known moments of the prior RV. For Gaussian priors, $\beta = 2$ is optimal. κ is a tertiary scaling factor and is usually set equal to 0. In general, the optimal values of these scaling parameters will be problem specific. For more detail on how to choose them, see Julier & Uhlmann.⁷
- *General notes:* The augmented state vector and sigma-point vector is given by $\mathbf{x}^a = \begin{bmatrix} \mathbf{x}^T & \mathbf{v}^T & \mathbf{n}^T \end{bmatrix}^T$, $\mathbf{x}^a = \begin{bmatrix} (\mathbf{x}^x)^T & (\mathbf{x}^v)^T & (\mathbf{x}^n)^T \end{bmatrix}$. \mathbf{R}_v and \mathbf{R}_n are the process-noise and observation-noise covariance matrices.
- *Linear-algebra operators* (See Golub^{5,38} for more detail): $\sqrt{\cdot}$: matrix square-root using lower triangular Cholesky decomposition.

B. Central Difference Kalman Filter (CDKF)

- *Initialization:*

$$\hat{\mathbf{x}}_0 = E[\mathbf{x}_0] \quad , \quad \mathbf{P}_{\mathbf{x}_0} = E[(\mathbf{x}_0 - \hat{\mathbf{x}}_0)(\mathbf{x}_0 - \hat{\mathbf{x}}_0)^T]$$

- *For $k = 1, \dots, \infty$:*

1. Set $t = k - 1$
2. Calculate sigma-points for time-update:

$$\begin{aligned}
\hat{\mathbf{x}}_t^{a_v} &= [\hat{\mathbf{x}}_t \quad \bar{\mathbf{v}}] \\
\mathbf{P}_t^{a_v} &= \begin{bmatrix} \mathbf{P}_{\mathbf{x}_{k-1}} & \mathbf{0} \\ \mathbf{0} & \mathbf{R}_v \end{bmatrix} \\
\mathbf{x}_t^{a_v} &= \begin{bmatrix} \hat{\mathbf{x}}_t^{a_v} & \hat{\mathbf{x}}_t^{a_v} + h\sqrt{\mathbf{P}_t^{a_v}} & \hat{\mathbf{x}}_t^{a_v} - h\sqrt{\mathbf{P}_t^{a_v}} \end{bmatrix}
\end{aligned}$$

3. Time-update equations:

$$\begin{aligned}
\mathbf{x}_{k|t}^x &= \mathbf{f}(\mathbf{x}_t^x, \mathbf{x}_t^v, \mathbf{u}_t) \\
\hat{\mathbf{x}}_k^- &= \sum_{i=0}^{2L} w_i^m \mathbf{x}_{i,k|t}^x \\
\mathbf{P}_{\mathbf{x}_k}^- &= \sum_{i=1}^L \left[w_i^{c1} (\mathbf{x}_{i,k|t}^x - \mathbf{x}_{L+i,k|t}^x)^2 + w_i^{c2} (\mathbf{x}_{i,k|t}^x + \mathbf{x}_{L+i,k|t}^x - 2\mathbf{x}_{0,k|t}^x)^2 \right]
\end{aligned}$$

4. Calculate sigma-points for measurement-update:

$$\begin{aligned}\hat{\mathbf{x}}_{k|t}^{a_n} &= [\hat{\mathbf{x}}_k^- \quad \bar{\mathbf{n}}] \\ \mathbf{P}_{k|t}^{a_n} &= \begin{bmatrix} \mathbf{P}_{\mathbf{x}_k}^- & \mathbf{0} \\ \mathbf{0} & \mathbf{R}_n \end{bmatrix} \\ \mathcal{X}_{k|t}^{a_n} &= \begin{bmatrix} \hat{\mathbf{x}}_{k|t}^{a_n} & \hat{\mathbf{x}}_{k|t}^{a_n} + h\sqrt{\mathbf{P}_{k|t}^{a_n}} & \hat{\mathbf{x}}_{k|t}^{a_n} - h\sqrt{\mathbf{P}_{k|t}^{a_n}} \end{bmatrix}\end{aligned}$$

5. Measurement-update equations:

$$\begin{aligned}\mathcal{Y}_{k|t} &= \mathbf{h}(\mathcal{X}_{k|t}^x, \mathcal{X}_{k|t}^n) \\ \hat{\mathbf{y}}_k^- &= \sum_{i=0}^{2L} w_i^m \mathcal{Y}_{i,k|t} \\ \mathbf{P}_{\tilde{\mathbf{y}}_k} &= \sum_{i=1}^L \left[w_i^{c_1} (\mathcal{Y}_{i,k|t} - \mathcal{Y}_{L+i,k|t})^2 + w_i^{c_2} (\mathcal{Y}_{i,k|t} + \mathcal{Y}_{L+i,k|t} - 2\mathcal{Y}_{0,k|t})^2 \right] \\ \mathbf{P}_{\mathbf{x}_k \mathcal{Y}_k} &= \sqrt{w_1^{c_1} \mathbf{P}_{\mathbf{x}_k}^-} [\mathcal{Y}_{1:L,k|t} - \mathcal{Y}_{L+1:2L,k|t}]^T \\ \mathbf{K}_k &= \mathbf{P}_{\mathbf{x}_k \mathcal{Y}_k} \mathbf{P}_{\tilde{\mathbf{y}}_k}^{-1} \\ \hat{\mathbf{x}}_k &= \hat{\mathbf{x}}_k^- + \mathbf{K}_k (\mathbf{y}_k - \hat{\mathbf{y}}_k^-) \\ \mathbf{P}_{\mathbf{x}_k} &= \mathbf{P}_{\mathbf{x}_k}^- - \mathbf{K}_k \mathbf{P}_{\tilde{\mathbf{y}}_k} \mathbf{K}_k^T\end{aligned}$$

- *Weights:* $w_0^m = (h^2 - L)/h^2$, $w_i^m = 1/(2h^2)$, $w_i^{c_1} = 1/(4h^2)$ and $w_i^{c_2} = (h^2 - 1)/(4h^4)$ for $i=1, \dots, 2L$ where $h \geq 1$ is the scalar central difference interval size which is optimally set equal to the square-root of the kurtosis of the prior random variable.² For Gaussian prior RVs, the optimal value is $h = \sqrt{3}$. The scaling factor h in the CDKF plays the same role of α in the UKF, i.e., it determines the spread of the sigma-points around the prior mean. L is the dimension of the augmented state vector.
- *General note:* Here we again augment the system state with the process noise and observation noise vectors (\mathbf{v}_k and \mathbf{n}_k) as we did for the UKF. For the CDKF, however, we split this augmentation between the time-update and measurement-update, i.e., for the time-update the augmented state vector and augmented covariance matrix is given by

$$\mathbf{x}_k^{a_v} = \begin{bmatrix} \mathbf{x}_k^T & \mathbf{v}_k^T \end{bmatrix}^T, \quad \mathbf{P}_k^{a_v} = \begin{bmatrix} \mathbf{P}_{\mathbf{x}_k} & \mathbf{0} \\ \mathbf{0} & \mathbf{R}_v \end{bmatrix},$$

and by

$$\mathbf{x}_k^{a_n} = \begin{bmatrix} \mathbf{x}_k^T & \mathbf{n}_k^T \end{bmatrix}^T, \quad \mathbf{P}_k^{a_n} = \begin{bmatrix} \mathbf{P}_{\mathbf{x}_k} & \mathbf{0} \\ \mathbf{0} & \mathbf{R}_n \end{bmatrix},$$

for the measurement-update. Accordingly the sigma-point vectors are given by: $\mathcal{X}^{a_v} = \begin{bmatrix} (\mathcal{X}^x)^T & (\mathcal{X}^v)^T \end{bmatrix}^T$ and $\mathcal{X}^{a_n} = \begin{bmatrix} (\mathcal{X}^x)^T & (\mathcal{X}^n)^T \end{bmatrix}^T$. Note: $(\cdot)^2$ is shorthand for the vector outer product, i.e., $\mathbf{a}^2 \doteq \mathbf{a}\mathbf{a}^T$.

C. Square-Root UKF (SRUKF)

- *Initialization:*

$$\begin{aligned}\hat{\mathbf{x}}_0 &= E[\mathbf{x}_0], \quad \mathbf{S}_{\mathbf{x}_0} = \sqrt{E[(\mathbf{x}_0 - \hat{\mathbf{x}}_0)(\mathbf{x}_0 - \hat{\mathbf{x}}_0)^T]} \\ \hat{\mathbf{x}}_0^a &= E[\mathbf{x}^a] = \begin{bmatrix} \hat{\mathbf{x}}_0 & \bar{\mathbf{v}} & \bar{\mathbf{n}} \end{bmatrix}^T \\ \mathbf{S}_0^a &= \sqrt{E[(\mathbf{x}_0^a - \hat{\mathbf{x}}_0^a)(\mathbf{x}_0^a - \hat{\mathbf{x}}_0^a)^T]} \\ &= \begin{bmatrix} \mathbf{S}_{\mathbf{x}_0} & \mathbf{0} & \mathbf{0} \\ \mathbf{0} & \mathbf{S}_v & \mathbf{0} \\ \mathbf{0} & \mathbf{0} & \mathbf{S}_n \end{bmatrix}\end{aligned}$$

- For $k = 1, \dots, \infty$:

1. Set $t = k - 1$
2. Calculate sigma-points:

$$\mathcal{X}_t^a = \begin{bmatrix} \hat{\mathbf{x}}_t^a & \hat{\mathbf{x}}_t^a + \gamma \mathbf{S}_{\mathbf{x}_t}^a & \hat{\mathbf{x}}_t^a - \gamma \mathbf{S}_{\mathbf{x}_t}^a \end{bmatrix}$$

3. Time-update equations:

$$\begin{aligned} \mathcal{X}_{k|t}^x &= \mathbf{f}(\mathcal{X}_t^a, \mathcal{X}_t^v, \mathbf{u}_t) \\ \hat{\mathbf{x}}_k^- &= \sum_{i=0}^{2L} w_i^m \mathcal{X}_{i,k|t}^x \\ \mathbf{S}_{\mathbf{x}_k}^- &= \text{qr} \left\{ \left[\sqrt{w_1^c} (\mathcal{X}_{1:2L,k|t}^x - \hat{\mathbf{x}}_k^-) \right] \right\} \\ \mathbf{S}_{\mathbf{x}_k}^- &= \text{cholupdate} \left\{ \mathbf{S}_{\mathbf{x}_k}^-, \mathcal{X}_{0,k|t}^x - \hat{\mathbf{x}}_k^-, w_0^{(c)} \right\} \\ \mathcal{Y}_{k|t} &= \mathbf{h}(\mathcal{X}_{i,k|t}^x, \mathcal{X}_t^n) \\ \hat{\mathbf{y}}_k^- &= \sum_{i=0}^{2L} w_i^m \mathcal{Y}_{i,k|t} \end{aligned}$$

4. Measurement-update equations:

$$\begin{aligned} \mathbf{S}_{\tilde{\mathbf{y}}_k} &= \text{qr} \left\{ \left[\sqrt{w_1^c} (\mathcal{Y}_{1:2L,k|t} - \hat{\mathbf{y}}_k^-) \right] \right\} \\ \mathbf{S}_{\tilde{\mathbf{y}}_k} &= \text{cholupdate} \left\{ \mathbf{S}_{\tilde{\mathbf{y}}_k}, \mathcal{Y}_{0,k|t} - \hat{\mathbf{y}}_k^-, w_0^{(c)} \right\} \\ \mathbf{P}_{\mathbf{x}_k \mathbf{y}_k} &= \sum_{i=0}^{2L} w_i^c (\mathcal{X}_{i,k|t}^x - \hat{\mathbf{x}}_k^-) (\mathcal{Y}_{i,k|t} - \hat{\mathbf{y}}_k^-)^T \\ \mathbf{K}_k &= \left(\mathbf{P}_{\mathbf{x}_k \mathbf{y}_k} / \mathbf{S}_{\tilde{\mathbf{y}}_k}^T \right) / \mathbf{S}_{\tilde{\mathbf{y}}_k} \\ \hat{\mathbf{x}}_k &= \hat{\mathbf{x}}_k^- + \mathbf{K}_k (\mathbf{y}_k - \hat{\mathbf{y}}_k^-) \\ \mathbf{U} &= \mathbf{K}_k \mathbf{S}_{\tilde{\mathbf{y}}_k} \\ \mathbf{S}_{\mathbf{x}_k} &= \text{cholupdate} \left\{ \mathbf{S}_{\mathbf{x}_k}^-, \mathbf{U}, -1 \right\} \end{aligned}$$

- *Weights & parameters:* $\gamma = \sqrt{L + \lambda}$, $w_0^m = \lambda / (L + \lambda)$, $w_0^c = w_0^m + (1 - \alpha^2 + \beta)$, $w_i^c = w_i^m = 1 / [2(L + \lambda)]$ for $i = 1, \dots, 2L$. $\lambda = \alpha^2(L + \kappa) - L$ is a compound scaling parameter, L is the dimension of the augmented state-vector, $0 < \alpha \leq 1$ is the primary scaling factor determining the extent of the spread of the sigma-points around the prior mean. Typical range for α is $1e-3 < \alpha \leq 1$. β is a secondary scaling factor used to emphasize the weighting on the zeroth sigma-point for the posterior covariance calculation. β can be used to minimize certain higher-order error terms based on known moments of the prior RV. For Gaussian priors, $\beta = 2$ is optimal. κ is a tertiary scaling factor and is usually set equal to 0. In general, the optimal values of these scaling parameters will be problem specific. For more detail on how to choose them, see Julier & Uhlmann.⁷
- *General notes:* The augmented state vector and sigma-point vector is given by $\mathbf{x}^a = \begin{bmatrix} \mathbf{x}^T & \mathbf{v}^T & \mathbf{n}^T \end{bmatrix}^T$, $\mathcal{X}^a = \begin{bmatrix} (\mathcal{X}^x)^T & (\mathcal{X}^v)^T & (\mathcal{X}^n)^T \end{bmatrix}$. $\mathbf{S}_v = \sqrt{\mathbf{R}_v}$ and $\mathbf{S}_n = \sqrt{\mathbf{R}_n}$ where \mathbf{R}_v and \mathbf{R}_n are the process-noise and observation-noise covariance matrices.
- *Linear-algebra operators* (see Golub³⁸ and Van der Merwe⁵ for more detail): $\sqrt{\cdot}$: matrix square-root using lower triangular Cholesky decomposition. $\text{qr}(\mathbf{A})$: lower-triangular part of \mathbf{R} matrix resulting from economy QR decomposition of data-matrix \mathbf{A} . $\text{cholupdate}\{\mathbf{R}, \mathbf{U}, \pm \nu\}$: N consecutive rank-1 Cholesky up(down)dates of the lower-triangular Cholesky factor \mathbf{R} by the N columns of $\sqrt{\nu} \mathbf{U}$. $/$: Efficient least-squares pseudo inverse implemented using triangular QR decomposition with pivoting.

D. Square-Root CDKF (SRCDKF)

- *Initialization:*

$$\hat{\mathbf{x}}_0 = E[\mathbf{x}_0] \quad , \quad \mathbf{S}_{\mathbf{x}_0} = \sqrt{E[(\mathbf{x}_0 - \hat{\mathbf{x}}_0)(\mathbf{x}_0 - \hat{\mathbf{x}}_0)^T]}$$

- For $k = 1, \dots, \infty$:

1. Set $t = k - 1$
2. Calculate sigma points for time-update:

$$\begin{aligned}\hat{\mathbf{x}}_t^{a_v} &= \begin{bmatrix} \hat{\mathbf{x}}_t & \bar{\mathbf{v}} \end{bmatrix}, \quad \mathbf{S}_t^{a_v} = \begin{bmatrix} \mathbf{S}_{\mathbf{x}_t} & \mathbf{0} \\ \mathbf{0} & \mathbf{S}_{\mathbf{v}} \end{bmatrix} \\ \mathcal{X}_t^{a_v} &= \begin{bmatrix} \hat{\mathbf{x}}_t^{a_v} & \hat{\mathbf{x}}_t^{a_v} + h\mathbf{S}_t^{a_v} & \hat{\mathbf{x}}_t^{a_v} - h\mathbf{S}_t^{a_v} \end{bmatrix}\end{aligned}$$

3. Time-update equations:

$$\begin{aligned}\mathcal{X}_{k|t}^x &= \mathbf{f}(\mathcal{X}_t^x, \mathcal{X}_t^v, \mathbf{u}_t) \\ \hat{\mathbf{x}}_k^- &= \sum_{i=0}^{2L} w_i^m \mathcal{X}_{i,k|t}^x \\ \mathbf{S}_{\mathbf{x}_k}^- &= \text{qr} \left\{ \left[\sqrt{w_1^{c_1}} (\mathcal{X}_{1:L,k|t}^x - \mathcal{X}_{L+1:2L,k|t}^x) \right. \right. \\ &\quad \left. \left. \sqrt{w_1^{c_2}} (\mathcal{X}_{1:L,k|t}^x + \mathcal{X}_{L+1:2L,k|t}^x - 2\mathcal{X}_{0,k|t}^x) \right] \right\}\end{aligned}$$

4. Calculate sigma-points for measurement update:

$$\begin{aligned}\hat{\mathbf{x}}_{k|t}^{a_n} &= \begin{bmatrix} \hat{\mathbf{x}}_k^- & \bar{\mathbf{n}} \end{bmatrix}, \quad \mathbf{S}_{k|t}^{a_n} = \begin{bmatrix} \mathbf{S}_{\mathbf{x}_k}^- & \mathbf{0} \\ \mathbf{0} & \mathbf{S}_{\mathbf{n}} \end{bmatrix} \\ \mathcal{X}_{k|t}^{a_n} &= \begin{bmatrix} \hat{\mathbf{x}}_{k|t}^{a_n} & \hat{\mathbf{x}}_{k|t}^{a_n} + h\mathbf{S}_{k|t}^{a_n} & \hat{\mathbf{x}}_{k|t}^{a_n} - h\mathbf{S}_{k|t}^{a_n} \end{bmatrix}\end{aligned}$$

5. Measurement-update equations:

$$\begin{aligned}\mathcal{Y}_{k|t} &= \mathbf{h}(\mathcal{X}_{k|t}^x, \mathcal{X}_{k|t}^n) \\ \hat{\mathbf{y}}_k^- &= \sum_{i=0}^{2L} w_i^m \mathcal{Y}_{i,k|t} \\ \mathbf{S}_{\tilde{\mathbf{y}}_k} &= \text{qr} \left\{ \left[\sqrt{w_1^{c_1}} (\mathcal{Y}_{1:L,k|t} - \mathcal{Y}_{L+1:2L,k|t}) \right. \right. \\ &\quad \left. \left. \sqrt{w_1^{c_2}} (\mathcal{Y}_{1:L,k|t} - \mathcal{Y}_{L+1:2L,k|t} - 2\mathcal{Y}_{0,k|t}) \right] \right\} \\ \mathbf{P}_{\mathbf{x}_k \mathbf{y}_k} &= \sqrt{w_1^{c_1}} \mathbf{S}_{\mathbf{x}_k}^- [\mathcal{Y}_{1:L,k|t} - \mathcal{Y}_{L+1:2L,k|t}]^T \\ \mathbf{K}_k &= (\mathbf{P}_{\mathbf{x}_k \mathbf{y}_k} / \mathbf{S}_{\tilde{\mathbf{y}}_k}^T) / \mathbf{S}_{\tilde{\mathbf{y}}_k} \\ \hat{\mathbf{x}}_k &= \hat{\mathbf{x}}_k^- + \mathbf{K}_k (\mathbf{y}_k - \hat{\mathbf{y}}_k^-) \\ \mathbf{U} &= \mathbf{K}_k \mathbf{S}_{\tilde{\mathbf{y}}_k} \\ \mathbf{S}_{\mathbf{x}_k} &= \text{cholupdate} \{ \mathbf{S}_{\mathbf{x}_k}^-, \mathbf{U}, -1 \}\end{aligned}$$

- *Weights*: $w_0^m = (h^2 - L)/h^2$, $w_i^m = 1/(2h^2)$, $w_i^{c_1} = 1/(4h^2)$ and $w_i^{c_2} = (h^2 - 1)/(4h^4)$ for $i=1, \dots, 2L$ where $h \geq 1$ is the scalar central difference interval size which is optimally set equal to the square-root of the kurtosis of the prior random variable.² For Gaussian prior RVs, the optimal value is $h = \sqrt{3}$. The scaling factor h in the CDKF plays the same role of α in the UKF, i.e., it determines the spread of the sigma-points around the prior mean. L is the dimension of the augmented state vector.
- *Other parameters*: $\mathbf{S}_{\mathbf{v}} = \sqrt{\mathbf{R}_{\mathbf{v}}}$ and $\mathbf{S}_{\mathbf{n}} = \sqrt{\mathbf{R}_{\mathbf{n}}}$ where $\mathbf{R}_{\mathbf{v}}$ and $\mathbf{R}_{\mathbf{n}}$ are the process-noise and observation-noise covariance matrices.
- *Linear-algebra operators* (see Golub³⁸ and Van der Merwe⁵ for more detail): $\sqrt{\cdot}$: matrix square-root using lower triangular Cholesky decomposition. $\text{qr}(\mathbf{A})$: lower-triangular part of \mathbf{R} matrix resulting from economy QR decomposition of data-matrix \mathbf{A} . $\text{cholupdate} \{ \mathbf{R}, \mathbf{U}, \pm \nu \}$: N consecutive rank-1 Cholesky up(down)dates of the lower-triangular Cholesky factor \mathbf{R} by the N columns of $\sqrt{\nu} \mathbf{U}$. $/$: Efficient least-squares pseudo inverse implemented using triangular QR decomposition with pivoting.

- *General note:* Here we again augment the system state with the process noise and observation noise vectors (\mathbf{v}_k and \mathbf{n}_k) as we did for the UKF. For the CDKF, however, we split this augmentation between the time-update and measurement-update, i.e., for the time-update the augmented state vector and augmented covariance matrix is given by

$$\mathbf{x}_k^{a_v} = \begin{bmatrix} \mathbf{x}_k^T & \mathbf{v}_k^T \end{bmatrix}^T, \quad \mathbf{P}_k^{a_v} = \begin{bmatrix} \mathbf{P}_{\mathbf{x}_k} & \mathbf{0} \\ \mathbf{0} & \mathbf{R}_v \end{bmatrix},$$

and by

$$\mathbf{x}_k^{a_n} = \begin{bmatrix} \mathbf{x}_k^T & \mathbf{n}_k^T \end{bmatrix}^T, \quad \mathbf{P}_k^{a_n} = \begin{bmatrix} \mathbf{P}_{\mathbf{x}_k} & \mathbf{0} \\ \mathbf{0} & \mathbf{R}_n \end{bmatrix},$$

for the measurement-update. Accordingly the sigma-point vectors are given by: $\mathcal{X}^{a_v} = \left[(\mathcal{X}^x)^T \quad (\mathcal{X}^v)^T \right]^T$ and $\mathcal{X}^{a_n} = \left[(\mathcal{X}^x)^T \quad (\mathcal{X}^n)^T \right]^T$. Note: $(\cdot)^2$ is shorthand for the vector outer product, i.e., $\mathbf{a}^2 \doteq \mathbf{a}\mathbf{a}^T$.

Appendix B: Sensor Latency Compensation - Fusing Lagged Measurements

When fusing latency delayed measurements with the current best prediction of the vehicle's state, care must be taken to incorporate this information in a mathematically correct fashion. Figure 11 demonstrates this issue graphically for a linear system given by

$$\mathbf{x}_{k+1} = \mathbf{A}_k \mathbf{x}_k + \mathbf{B}_k \mathbf{u}_k + \mathbf{v}_k \quad (55)$$

$$\mathbf{y}_k = \mathbf{C}_k \mathbf{x}_k + \mathbf{n}_k, \quad (56)$$

where $\mathbf{v}_k \sim N(\mathbf{0}, \mathbf{R}_v)$ and $\mathbf{n}_k \sim N(\mathbf{0}, \mathbf{R}_n)$. The state estimation filter, in general, receives measurements from a variety of sensors at each measurement-update step. Some measurements corresponds to the system state at the current time, \mathbf{y}_k , given by Equation 56, while other latency-delayed measurements, \mathbf{y}_k^* , correspond to the system state at time $l = k - N$, i.e.,

$$\mathbf{y}_k^* = \mathbf{C}_l^* \mathbf{x}_l + \mathbf{n}_k^*,$$

where N is the sensor latency measured in sample periods, \mathbf{C}_l^* is the measurement sensitivity matrix and \mathbf{n}_k^* is the observation noise for the delayed measurement with $\mathbf{n}_k^* \sim N(\mathbf{0}, \mathbf{R}_n^*)$. The challenge now is this: how do we optimally fuse these different sets of measurements with the current estimate of the system state?

A number of different solutions to the sensor latency problem has been suggested in the literature^{9,39,40} for application to *linear* systems through the use of modified linear Kalman filters. We will now briefly review these different approaches.

The simplest to implement, but also the most inaccurate, solution is to simply ignore the fact that the sensor measurement is lagged. A normal Kalman measurement update is then performed to fuse the delayed sensor measurement with the current state estimate. This is the option that was used for the GPS sensor fusion in MIT's EKF based UAV state estimator.³¹ Their rationale was that the 50ms latency of the Ashtech G12 GPS receiver was short enough to not cause significant errors if ignored.⁴¹ Even though this assumption is probably reasonable for the specific time-delay at hand, we felt that valuable information in the measurements were still being discarded using this approach and that compensating for the latency will in fact result in a significant increase in estimation performance. This was experimentally confirmed earlier in the Experimental Results section.

Another approach used to compensate for measurement latency is to simply recalculate the complete time-trajectory of the filter through the delay period, when a lagged measurement is received. This requires all of the observations (both lagged and non-lagged) as well as the system state estimates to be saved for the complete latency duration, i.e. $\tilde{k} \in [k - N, k - N + 1, \dots, k - 1, k]$. Not only does this incur a large storage cost for any significant sensor latency, but the computational burden also increases rapidly as the recalculation period becomes longer. This has serious implications if the filter rate is such that new state estimates has to be calculated within a short period of time. The only advantage of this approach is that the resulting state estimates will be exact (for linear systems), i.e., no approximations with regard to the sensor latency has been made. Unfortunately, due to the large storage and computational cost, this method is almost never employed.

Another typical approximate solution used to deal with this latency problem is to store the value of the state estimate corresponding to the latency-lagged sensor measurement, i.e., $\hat{\mathbf{x}}_{k-N}$, in a buffer. When the

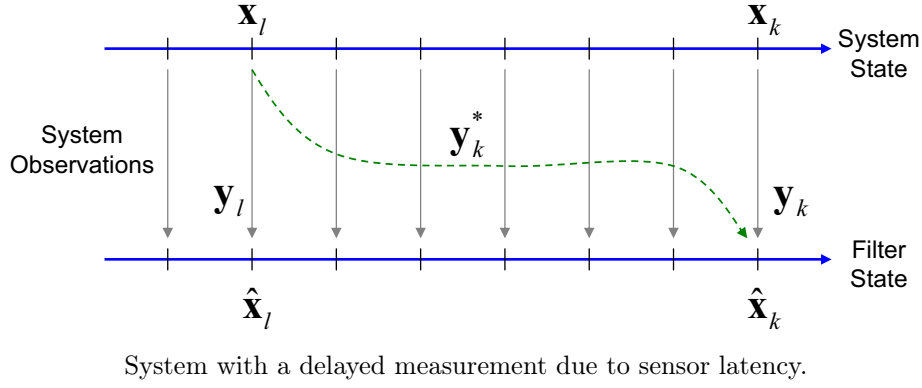


Figure 11. **System with a delayed measurement due to sensor latency:** At time k the state estimation filter receives two sets of sensor measurements from the system: A normal measurement \mathbf{y}_k corresponding to the system state at time k , as well as a delayed measurement \mathbf{y}_k^* corresponding to the system state at time $l = k - N$, where N is the sensor latency (measured in sample periods).

lagged measurement \mathbf{y}_k^* then eventually becomes available at time k , the “prediction of the observation”, $\hat{\mathbf{y}}_k^{*-}$, is calculated using the correct lagged state estimate $\hat{\mathbf{x}}_{k-N}$, i.e.

$$\hat{\mathbf{y}}_k^{*-} = \mathbf{C}_{k-N}^* \hat{\mathbf{x}}_{k-N} . \quad (57)$$

The innovation based on this lagged prediction, $\mathbf{y}_k^* - \hat{\mathbf{y}}_k^{*-}$, is then fused using the standard Kalman measurement-update with the *current* predicted state, i.e.

$$\hat{\mathbf{x}}_k = \hat{\mathbf{x}}_k^- + \mathbf{K} (\mathbf{y}_k^* - \hat{\mathbf{y}}_k^{*-}) . \quad (58)$$

Since the correct innovation is fused with the wrong state prediction, this method although better than the first approach, is still sub-optimal.

In Alexander,³⁹ a method is derived where it suffices to calculate a correction term which is then added to the filter estimates when the latency-delayed measurements arrive. Referring to the standard Kalman filter equations (Equations 3-7) and Figure 11, the measurement \mathbf{y}_l should be fused at time $l = k - N$, causing a correction in the state estimate $\hat{\mathbf{x}}_l^-$ and a decrease in the state covariance $\mathbf{P}_{\mathbf{x}_l}^-$. As the Kalman gain is a function of this updated state covariance, the measurements occurring after this time ($k > l$) will all be fused differently than if the measurement update for \mathbf{y}_k^* is omitted. If therefore the measurement \mathbf{y}_l is delayed by N samples (resulting in \mathbf{y}_k^*) and fused at time k , the data update should reflect the fact that the N data updates from time l to k , and therefore the state and covariance estimates, have all been affected by the delay in a complex manner.⁹ Equations that account for this when fusing \mathbf{y}_k^* at time k were derived³⁹ but are of such complexity that they are practically infeasible for most applications^d. This approach was reformulated into a practically implementable method (called *Larsen's method*⁹) which does, however, require (at time l) the measurement sensitivity matrix \mathbf{C}_l^* and the observation noise covariance matrix \mathbf{R}_n^* to be known at time l (which is often the case). If these requirements are met, the filter covariance should be updated at time l as if the measurement \mathbf{y}_k^* is already available. This leads the measurements in the delay period to be fused as if \mathbf{y}_k^* had been fused at time l . At time k , when \mathbf{y}_k^* actually becomes available, incorporating the measurement (\mathbf{y}_k^*) correctly is then greatly simplified, by adding the following correction term after the non-lagged observation \mathbf{y}_k has been fused:

$$\delta \hat{\mathbf{x}}_k = \mathbf{M}_* \mathbf{K}_l (\mathbf{y}_k^* - \mathbf{C}_l^* \hat{\mathbf{x}}_l) \quad (59)$$

If the latency delay is zero, \mathbf{M}_* is the identity matrix. For $N > 0$, \mathbf{M}_* is given by:

$$\mathbf{M}_* = \prod_{i=0}^{N-1} \left(\mathbf{I} - \mathbf{K}_{k-i}' \mathbf{C}_{k-i} \right) \mathbf{A}_{k-i-1} , \quad (60)$$

^dIn fact, the computational complexity is comparable to recalculating the complete Kalman filter through the complete delay of N_{lag} samples,⁹ which is equivalent to the previously discussed exact method for latency compensation.

where \mathbf{K}' signifies Kalman gain matrices that have been calculated based on a covariance matrix updated at time l with the covariance of the delayed measurement^e. This implies that the covariance estimates of the filter will be wrong in a period of N samples (before the delayed measurement arrives), causing normal non-delayed measurements during this period to be fused sub-optimally. However, after the correction term (Equation 59) is added, the filter state and covariance will once again be optimal. Take note that Equations 60 and 59 assumes a linear dynamic state-space model.

Larsen⁹ extended the previous approach further to a method that provides optimally fused estimates not only at the instances when the delayed measurements arrive, but also during the interim period between these updates. This is achieved by running a second parallel Kalman filter that generates optimal estimates in the interim (between delayed measurements) period: At time l the first filter is updated according to Larsen's first method (shown above) incorporating the covariance of the not-yet-received delayed measurement \mathbf{y}_k^* . This filter, will generate non-optimal estimates *until* the delayed measurement is actually received, but it will build up the correct terms needed for an optimal measurement update at that time. During this interim period the second filter, which was not pre-updated at time l , will generate optimal estimates when fusing non-delayed measurements. At time k , the correctly fused optimal estimate of the first filter (which incorporated the delayed measurement) and its covariance is used to reinitialize the second filter. Using this approach optimal estimates are available at all times. The downside is that two Kalman filters need to be run in parallel which will double the computational complexity.

Of the approaches discussed above, *Larsen's modified two-filter method* is the only approach that is both computationally practical and produces optimal states estimates at all time. *The method is, however, only exact for linear systems.* For nonlinear systems, the recursive calculation of the corrections terms (Equations 60 and 59) must be approximated through the use of linearized system matrices. If the linearization errors are severe, it is expected that large errors may accumulate over time resulting in sub-optimal corrections when the lagged measurements finally arrive.

E. SPKF Based Time Delayed Sensor Fusion

In this section, we introduce an alternative approach for optimally fusing latency delayed sensor data in *general nonlinear* systems. In order to accurately fuse a N -sample *lagged* innovation vector

$$\tilde{\mathbf{y}}_{k-N} = \mathbf{y}_{k-N} - \hat{\mathbf{y}}_{k-N}^- \quad (61)$$

with the *current* prediction of the system state $\hat{\mathbf{x}}_k^-$, the Kalman update formulation of Eq. (3) is re-written as

$$\hat{\mathbf{x}}_k = \hat{\mathbf{x}}_k^- + \tilde{\mathbf{K}}_{k,N} \tilde{\mathbf{y}}_{k-N} . \quad (62)$$

In Eq. (62) the Kalman gain is again expressed in terms of the correct covariance terms, i.e.,

$$\tilde{\mathbf{K}}_{k,N} = \mathbf{P}_{\mathbf{x}_k \tilde{\mathbf{y}}_{k-N}} \mathbf{P}_{\tilde{\mathbf{y}}_{k-N}}^{-1} , \quad (63)$$

where $\mathbf{P}_{\mathbf{x}_k \tilde{\mathbf{y}}_{k-N}}$ and $\mathbf{P}_{\tilde{\mathbf{y}}_{k-N}}$ are calculated by propagating sigma-points drawn from $\mathbf{P}_{\mathbf{x}_k \mathbf{x}_{k-N}}$ and $\mathbf{P}_{\mathbf{x}_{k-N}}$ (and corresponding lagged mean $\hat{\mathbf{x}}_{k-N}$) through the observation function $\mathbf{h}(\cdot)$ and applying the standard SPKF covariance calculation formulation of Eqs. (22) and (21). The optimal lagged observation prediction is given by

$$\hat{\mathbf{y}}_{k-N}^- = E [\mathbf{h}(\hat{\mathbf{x}}_{k-N}^-, \mathbf{n}_{k-N})] \quad (64)$$

which is also calculated using the standard sigma-point propagation technique of Eq. (20) after sigma-points were drawn from $\{\hat{\mathbf{x}}_{k-N}, \mathbf{P}_{\mathbf{x}_{k-N}}\}$.

The key insight here is that we need to accurately maintain the lagged state estimate $\hat{\mathbf{x}}_{k-N}$ as well as the correct lagged covariance and cross-covariance estimates $\mathbf{P}_{\mathbf{x}_k \mathbf{x}_{k-N}}$ and $\mathbf{P}_{\mathbf{x}_{k-N}}$ within the SPKF as the system evolves from time $k-N$ to the current time k . Note that $\mathbf{P}_{\mathbf{x}_k \mathbf{x}_{k-N}}$ corresponds to the cross-covariance-over-time between the system state at time $k-N$ and the current time k , i.e., $\mathbf{P}_{\mathbf{x}_k \mathbf{x}_{k-N}} = E[(\mathbf{x}_k - \hat{\mathbf{x}}_k^-)(\mathbf{x}_{k-N} - \hat{\mathbf{x}}_{k-N}^-)^T]$. One approximate method to do this was shown above, based on recursively applying the linearized system model to propagate the needed covariance term (see Equations 59 and 60). We will now present an alternative method to maintain the cross-covariance term through augmentation of the system state and redefinition of the process model.

^eSince the covariance update only depends on \mathbf{C}_l^* and \mathbf{R}_n^* and not \mathbf{y}_k^* , it can be precalculated.

This can be achieved within the SPKF framework by augmenting the state vector at time $k - N$ with the lagged state $\mathbf{x}_{lag} = \mathbf{x}_{k-N}$, i.e.,

$$\mathbf{x}_{k-N}^{(a)} = \begin{bmatrix} \mathbf{x}_{k-N} \\ \mathbf{x}_{lag} \end{bmatrix} \quad (65)$$

and then redefining the process models as

$$\begin{aligned} \mathbf{x}_{k-N+1}^{(a)} &= \check{\mathbf{f}} \left(\mathbf{x}_{k-N}^{(a)}, \mathbf{v}_{k-N} \right) \\ &= \begin{bmatrix} \mathbf{f} \left(\mathbf{x}_{k-N}, \mathbf{v}_{k-N} \right) \\ \mathbf{x}_{lag} \end{bmatrix} \\ &= \begin{bmatrix} \mathbf{x}_{k-N+1} \\ \mathbf{x}_{lag} \end{bmatrix} \end{aligned} \quad (66)$$

and the observation model (which is only valid at time k) by

$$\begin{aligned} \mathbf{y}_k^* &= \check{\mathbf{h}}_1 \left(\mathbf{x}_k^{(a)}, \mathbf{n}_k^{(a)} \right) \\ &= \mathbf{h} \left(\mathbf{x}_{lag}, \mathbf{n}_{lag} \right) \\ &= \mathbf{h} \left(\mathbf{x}_{k-N}, \mathbf{n}_{k-N} \right) \end{aligned} \quad (67)$$

for the lagged measurements, and by

$$\begin{aligned} \mathbf{y}_k &= \check{\mathbf{h}}_2 \left(\mathbf{x}_k^{(a)}, \mathbf{n}_k^{(a)} \right) \\ &= \mathbf{h} \left(\mathbf{x}_k, \mathbf{n}_k \right) \end{aligned} \quad (68)$$

for normal (non-delayed) measurements. Note, the augmented process model (Equations 66) updates the first component of the augmented state using the original process model while keeping the second component, \mathbf{x}_{lag} , constant. This approach will thus maintain the value of the system state at some prior point in time and update the current state of the system. Further note that $\mathbf{y}_k^* = \mathbf{y}_{k-N}$, i.e., an observation of the system state at time $k - N$ which is received at time k . Using this redefined state and process model from time $k - N$ to k within the normal SPKF framework will result in the following prediction of the state mean and covariance at time k , just before the lagged measurement is fused:

$$\begin{aligned} \hat{\mathbf{x}}_k^{(a)-} &= \begin{bmatrix} \hat{\mathbf{x}}_k^- \\ \hat{\mathbf{x}}_{lag}^- \end{bmatrix} = \begin{bmatrix} \hat{\mathbf{x}}_k^- \\ \hat{\mathbf{x}}_{k-N}^- \end{bmatrix} \\ \mathbf{P}_{\mathbf{x}_k}^- &= \begin{bmatrix} \mathbf{P}_{\mathbf{x}_k}^- & \mathbf{P}_{\mathbf{x}_k \mathbf{x}_{lag}}^- \\ \mathbf{P}_{\mathbf{x}_{lag} \mathbf{x}_k}^- & \mathbf{P}_{\mathbf{x}_{lag}}^- \end{bmatrix} = \begin{bmatrix} \mathbf{P}_{\mathbf{x}_k}^- & \mathbf{P}_{\mathbf{x}_k \mathbf{x}_{k-N}}^- \\ \mathbf{P}_{\mathbf{x}_{k-N} \mathbf{x}_k}^- & \mathbf{P}_{\mathbf{x}_{k-N}}^- \end{bmatrix} \end{aligned}$$

Sigma-points are now drawn from this prior distribution of the augmented state and propagated through the redefined observation model (Eq. (67)) in order to calculate

$$\mathbf{P}_{\mathbf{x}_k^{(a)} \tilde{\mathbf{y}}_{k-N}} = \begin{bmatrix} \mathbf{P}_{\mathbf{x}_k \tilde{\mathbf{y}}_{k-N}}^T & \mathbf{P}_{\mathbf{x}_{k-N} \tilde{\mathbf{y}}_{k-N}}^T \end{bmatrix}^T$$

and $\mathbf{P}_{\tilde{\mathbf{y}}_{k-N}}$ using the standard SPKF framework of Eqs. (22) and (21). These terms can then be used to compute the correct Kalman gain

$$\tilde{\mathbf{K}}_{k,N} = \mathbf{P}_{\mathbf{x}_k^{(a)} \tilde{\mathbf{y}}_{k-N}} \mathbf{P}_{\tilde{\mathbf{y}}_{k-N}}^{-1} = \begin{bmatrix} \mathbf{P}_{\mathbf{x}_k \tilde{\mathbf{y}}_{k-N}} \mathbf{P}_{\tilde{\mathbf{y}}_{k-N}}^{-1} \\ \mathbf{P}_{\mathbf{x}_{k-N} \tilde{\mathbf{y}}_{k-N}} \mathbf{P}_{\tilde{\mathbf{y}}_{k-N}}^{-1} \end{bmatrix}$$

needed to fuse the lagged measurement when it is received at time k .

An additional issue to be dealt with is how to update the augmented state during the latency period when a normal (non time delayed) measurement arrives. For example, while the system is waiting for a lagged

sensor (e.g. GPS) to output its measurement of the system state at time $k - N$, it receives a non-lagged measurement from another sensor (e.g. altimeter), which must now be fused with the current estimate of the system state. One solution to this problem is through the use of the *Schmidt-Kalman filter*.⁴² This alternate formulation of the Kalman filter has the property that certain states are marked as “ancillary” whose values are not updated. It uses the *Joseph form*⁴³ of the measurement update equations and a modified Kalman gain equation given by

$$\tilde{\mathbf{K}}_{k,N} = \mathbf{M} \mathbf{P}_{\mathbf{x}_k^{(a)} \tilde{\mathbf{y}}_{k-N}} \mathbf{P}_{\tilde{\mathbf{y}}_{k-N}}^{-1}, \quad (69)$$

where \mathbf{M} is the indicator matrix that indicates which of the states must be updated and which are “ancillary”. It is block diagonal with 1s in the diagonals for states which are updated and 0s for states which are not to be updated. For our specific case at hand, \mathbf{M} is given by

$$\mathbf{M} = \begin{bmatrix} \mathbf{I} & \mathbf{0} \\ \mathbf{0} & \mathbf{0} \end{bmatrix}. \quad (70)$$

A second solution we propose, is to use a normal Kalman measurement update without the use of the indicator matrix \mathbf{M} and ancillary (non updated) states. The result of this will be that the original state estimate, \mathbf{x}_{lag} in the augmented state vector (Equation 65) will no longer stay constant throughout the latency period due to the measurement update performed on it. It will now be measurement-updated based on subsequent information that has been observed. This deviates from Larsen’s method⁹ and should give better results. In fact, what will happen is that the original state estimate \mathbf{x}_l (from which the delayed sensor measurement is derived), will be *improved* during the latency period using future non-delayed observations. This can be thought of as a *smoothing operations*. Here we use the term *smoothing* to simply imply that past estimates of the system state can somehow be improved based on subsequent future observations of measurement data. This is a well known result from signal-processing filter theory.⁴⁴ Since we are waiting for the lagged sensor during the latency period, data received in the interim can be used to improve our estimate of the system state that the sensor will eventually be reporting on. When the delayed measurement then finally arrives and the innovation is calculated using Equation 61, the prediction of the delayed observation will be more accurate since it will now be calculated using the improved lagged state estimate. For a more detailed exposition of this method see Van der Merwe.⁵

The advantage of the SPKF formulation for fusing time-delayed sensor measurements (as presented above), is that the latency delayed measurements are incorporated using the exact same algorithmic framework used to recursively estimate the normal states. The latency compensation framework benefits in the same way from the second-order accuracy of the sigma-point approach. The disadvantage of this method, compared to some of the simpler approximate methods, is that the state dimension (and hence the number of sigma-points) doubles during the sensor latency period, resulting in an increase in computational complexity.

Acknowledgements

This work was supported in part by the following grants: NSF ECS-0083106 & ONR-FNC N0014-02-C-0248. The authors would like to thank Dr. Alexander Bogdanov, Geoff Harvey, and John Hunt for assistance with the UAV platform and data collection.

References

- ¹S. Julier, J. Uhlmann, and H. Durrant-Whyte, “A new approach for filtering nonlinear systems,” in *Proceedings of the American Control Conference*, pp. 1628–1632, 1995.
- ²M. Norgaard, N. Poulsen, and O. Ravn, “New Developments in State Estimation for Nonlinear Systems,” *Automatica*, vol. 36, pp. 1627–1638, November 2000.
- ³R. van der Merwe and E. Wan, “Efficient Derivative-Free Kalman Filters for Online Learning,” in *Proceedings of the 9th European Symposium on Artificial Neural Networks (ESANN)*, (Bruges, Belgium), pp. 205–210, Apr 2001.
- ⁴R. van der Merwe and E. Wan, “The Square-Root Unscented Kalman Filter for State- and Parameter-Estimation,” in *Proceedings of the IEEE International Conference on Acoustics, Speech, and Signal Processing (ICASSP)*, vol. 6, (Salt Lake City, UT), pp. 3461–3464, May 2001.
- ⁵R. van der Merwe, *Sigma-Point Kalman Filters for Probabilistic Inference in Dynamic State-Space Models*. PhD thesis, OGI School of Science & Engineering at Oregon Health & Science University, Portland, OR, April 2004.
- ⁶R. van der Merwe, “Sigma-Point Kalman Filters for Probabilistic Inference in Dynamic State-Space Models,” in *Workshop on Advances in Machine Learning*, (Montreal), June 2003. <http://www.iro.umontreal.ca/~kegl/CRMWorkshop/program.html>.
- ⁷S. J. Julier and J. K. Uhlmann, “Unscented Filtering and Nonlinear Estimation,” *Proceedings of the IEEE*, vol. 92, pp. 401–422, March 2004.

- ⁸E. A. Wan and R. van der Merwe, "The Unscented Kalman Filter for Nonlinear Estimation," in *Proceedings of IEEE Symposium on Adaptive Systems for Signal Processing Communications and Control (AS-SPCC)*, (Lake Louise, Alberta, Canada), pp. 153–158, October 2000.
- ⁹T. D. Larsen, N. A. Andersen, and O. Ravn, "Incorporation of Time Delayed Measurements in a Discrete-time Kalman Filter," in *Proceedings of the 37th IEEE Conference on Decision & Control*, (Tampa, Florida, USA), pp. 3972–3977, Dec 1998.
- ¹⁰F. L. Lewis, *Optimal Estimation*. New York: John Wiley & Sons, Inc., 1986.
- ¹¹S. J. Julier and J. K. Uhlmann, "A New Extension of the Kalman Filter to Nonlinear Systems," in *Proc. SPIE - Int. Soc. Opt. Eng. (USA)*, vol. 3068, (Orlando, FL), pp. 182–193, April 1997.
- ¹²S. Haykin, ed., *Kalman Filtering and Neural Networks*, ch. 7 - The Unscented Kalman Filter, E. A. Wan and R. van der Merwe, pp. 221–280. Adaptive and Learning Systems for Signal Processing, Communications, and Control, Wiley, 2001.
- ¹³S. Haykin, *Neural Networks : A Comprehensive Foundation*. Englewood Cliffs, NJ: Macmillan College Publishing Company, Inc, 1994.
- ¹⁴C. M. Bishop, *Neural Networks for Pattern Recognition*. Oxford University Press, 1995.
- ¹⁵S. Brunke and M. E. Campbell, "Estimation Architecture for Future Autonomous Vehicles," in *Proceedings of the American Control Conference*, (Anchorage, AK), pp. 1108–1114, AIAA, 2002.
- ¹⁶L. Mihaylova, J. De Schutter, and H. Bruyninckx, "A Multisine Approach for Trajectory Optimization Based on Information Gain," in *Proceedings of IEEE International Conference on Intelligent Robots and Systems*, (Lauzanne, Switzerland), pp. 661–666, September 2002.
- ¹⁷M. Niculescu, "Use of spkf in crista uav autopilot." Private Communications, Jan 2004. <http://www.cloudcaptech.com>.
- ¹⁸N. Cui, L. Hong, and J. R. Layne, "A Comparison of Nonlinear Filtering Approaches with Application to Ground Target Tracking," *Signal Processing (EURASIP/Elsevier)*, 2003.
- ¹⁹M. N. Andersen, R. O. Andersen, and K. Wheeler, "Filtering in Hybrid Dynamic Bayesian Networks," in *Proceedings of IEEE International Conference on Acoustics, Speech, and Signal Processing (ICASSP)*, (Montreal, Canada), pp. 773–776, May 2004.
- ²⁰Y. Chen, T. Huang, and Y. rui, "Parametric Contour Tracking using the Unscented Kalman Filter," in *Proceedings of the International Conference on Image Processing (ICIP)*, vol. 3, pp. 613–616, 2002.
- ²¹Y. Rui and Y. Chen, "Better Proposal Distributions: Object Tracking Using Unscented Particle Filter," in *Proc. of IEEE CVPR*, vol. II, (Kauai, Hawaii), pp. 786–793, Dec 2001.
- ²²P. Li and T. Zhang, "Visual Contour Tracking Based on Particle Filters," in *Proceedings of the First International Workshop on Generative-Model-Based Vision (GMBV)*, (Copenhagen), pp. 61–70, June 2002. <http://www.diku.dk/publikationer/tekniske.rapper/2002/02-01/> [Viewed: July 31, 2003].
- ²³M. E. Irwin, N. Cressie, and G. Johannesson, "Spatial-Temporal Nonlinear Filtering Based on Hierarchical Statistical Models," *Sociedad de Estadística e Investigación Operativa : Test*, vol. 11, no. 2, pp. 249–302, 2002.
- ²⁴E.-H. Shin and N. El-Sheimy, "An Unscented Kalman Filter for In-Motion Alignment of Low-Cost IMUs," in *Proceedings of the IEEE Frames Conference*, (Monterey, California), pp. 273–279, April 2004.
- ²⁵M. C. Mackey and L. Glass, "Oscillation and chaos in a physiological control system," *Science*, vol. 197, pp. 287–289, June 1977.
- ²⁶A. Lapedes and R. Farber, "Nonlinear Signal Processing using Neural Networks: Prediction and System modelling," Tech. Rep. LAUR872662, Los Alamos National Laboratory, 1987.
- ²⁷J. R. Cloutier, C. N. D'Souza, and C. P. Mracek, "Nonlinear regulation and nonlinear H-infinity control via the state-dependent Riccati equation technique: Part1, Theory,," in *Proceedings of the International Conference on Nonlinear Problems in Aviation and Aerospace*, (Daytona Beach, FL), pp. 117–130, May 1996.
- ²⁸E. Feron, "Aerial robotics project : Laboratory for information and decision systems mit." <http://gewurtz.mit.edu/research/heli.htm>.
- ²⁹A. A. Bogdanov, E. A. Wan, M. Carlsson, R. Kiebertz, G. Harvey, J. Hunt, and R. van der Merwe, "State-Dependent Ricatti Equation Control of a Small Unmanned Helicopter," in *Proceedings of the AIAA Guidance Navigation and Control Conference*, (Austin, TX), August 2003. AIAA Paper Number: 2003-5672.
- ³⁰A. A. Bogdanov and E. A. Wan, "SDRE Control with Nonlinear Feedforward Compensation for a Small Unmanned Helicopter," in *Proceedings of the 2nd AIAA Unmanned Unlimited Systems, Technologies, and Operations Conference*, (San Diego, CA), September 2003. AIAA Paper Number: 2003-6512.
- ³¹V. Gavrillets, *Autonomous Aerobatic Maneuvering of Miniature Helicopters: Modeling and Control*. PhD thesis, Massachusetts Institute of Technology, Cambridge, MA, 2003.
- ³²P. G. Savage, "Strapdown Inertial Navigation Integration Algorithm Design Part 1: Attitude Algorithms," *Journal of Guidance, Control, and Dynamics*, vol. 21, pp. 19–28, Jan 1998.
- ³³P. G. Savage, "Strapdown Inertial Navigation Integration Algorithm Design Part 2: Velocity and Position Algorithms," *Journal of Guidance, Control, and Dynamics*, vol. 21, pp. 208–221, March 1998.
- ³⁴B. Stevens and F. Lewis, *Aircraft Control and Simulation*. New York, NY: Wiley, 1992.
- ³⁵S. Nassar, K. Schwarz, and N. El-Sheimy, "INS and INS/GPS Accuracy Improvement Using Autoregressive (AR) Modeling of INS Sensor Errors," in *Proceedings of ION-NTM*, (San Diego), pp. 936–944, Jan 2004.
- ³⁶J. M. Rolfe and K. J. Staples, *Flight Simulation*. United Kingdom: Cambridge University Press, 1986.
- ³⁷K. Ito and K. Xiong, "Gaussian Filters for Nonlinear Filtering Problems," *IEEE Transactions on Automatic Control*, vol. 45, pp. 910–927, May 2000.
- ³⁸G. H. Golub and van Loan C. F., *Matrix Computations*. Johns Hopkins University Press, 1996.
- ³⁹H. L. Alexander, "State Estimation for Distributed Systems with Sensing Delay," *SPIE : Data Structures and Target Classification*, vol. 1470, pp. 103–111, 1991.
- ⁴⁰M. Bak, T. D. Larsen, M. Norgaard, N. A. Andersen, N. K. Poulsen, and O. Ravn, "Location Estimation using Delayed Measurements," in *Proceedings of the 5th International Workshop on Advanced Motion Control (AMC98)*, (Coimbra, Portugal), pp. 180–185, June 1998.
- ⁴¹V. Gavrillets, "MIT X-Cell-60 UAV Platform EKF Estimator." Private Communications, February 2003.
- ⁴²S. F. Schmidt, C. T. Leondes, editor, *Advances in Control Systems*, vol. 3, ch. Applications of State Space Methods to Navigation Problems, pp. 293–340. Academic Press, 1966.
- ⁴³A. Gelb, ed., *Applied Optimal Estimation*. MIT Press, 1974.
- ⁴⁴S. Haykin, *Adaptive Filter Theory*. Prentice-Hall, Inc, 3 ed., 1996.